

Smart Design of Noble Metal–Copper Chalcogenide Dual Plasmonic Heteronanoarchitectures for Emerging Applications: Progress and Prospects

Mariia Ivanchenko and Hao Jing*



Cite This: *Chem. Mater.* 2023, 35, 4598–4620



Read Online

ACCESS |

Metrics & More

Article Recommendations

ABSTRACT: Dual plasmonic metal–semiconductor heteronanostructures have been actively investigated due to their outstanding functional characteristics arising from the merging of two materials. In this review, the synthetic approaches, various designs, enhanced properties, and prospective applications of noble metal–nonstoichiometric copper chalcogenide nanosystems are summarized. The tunable size, shape, structure type (solid or hollow), composition, and doping level of the constituents produce several configurations of heteronanocomposites reported here. The colloidal synthetic approaches for the fabrication of dual plasmonic nanomaterials with controllable plasmonic properties are presented as well. The unique features of dual plasmonic nanostructures show synergistic and plasmon resonance coupling effects and enhanced light–matter interactions, which cannot be simply assigned to the mixture of pristine materials. Dual plasmonic hybrid nanosystems are promising candidates for enhanced photocatalysis, photothermal cancer therapy, improved sensing, photovoltaic devices, and upconversion luminescence. In conclusion, a brief outlook of the identified challenges in the area of dual plasmonic noble metal–vacancy-doped copper chalcogenide nanomaterials to be addressed in the nearest future is provided.



1. INTRODUCTION

The merger of various nanocrystals into one entity is attracting more and more attention because of the capabilities of such hybrid nanosystems, which often outperform the pristine NPs. Among various hybrid nanostructures, nanocomposites are formed by integrating the noble metal with heavily doped n- or p-type semiconductors, where both constituents possess plasmonic properties and demonstrate far superior physicochemical characteristics corresponding to the synergistic effects due to coupling between two different counterparts.^{1–4} While plasmonic properties of sole metallic nanoparticles, such as silver (Ag) and gold (Au), have been studied profoundly over several decades,⁵ the investigation of localized surface plasmon resonances (LSPRs) in semiconductors was pioneered by Zhao et al. in 2009.⁶ Now, it is known that any semiconductor NP with a sufficient free carrier density can sustain LSPRs.⁷ Unlike metallic nanoparticles, a semiconductor LSPR can be easily tuned from the visible region to the terahertz region, depending on the degree of doping, size, and geometry of the NP. The required concentration of free charges is reached by the formation of vacancies, named intrinsic doping, or substitution with heterovalent dopant atoms, also called extrinsic doping.⁸ Based on the doping type, plasmonic semiconductor nanomaterials could be classified as self-doped copper chalcogenides Cu_{2-x}E (E = S, Se, Te), molybdenum/tungsten oxides (MoO_{3-x} , WO_{3-x}), and doped metal oxides (Sn-doped In_2O_3). The heterointegration of multiple optically

active components at the nanoscale can create a new generation of integrated nanosystems with unprecedented performance or unique functions to break the boundaries of traditional technologies.⁹ Due to the changes in their architectures or surrounding media, plasmonic heteronano-composites exhibit extraordinary tunability of extinction and broaden the light response from the UV–visible spectrum to the NIR region, which makes up approximately 50% of the solar-light energy.

In this review, we focus on the recent advances in the synthesis of noble metal–nonstoichiometric copper chalcogenide heteronanostructures of various structural architecture and their plasmonic behavior. Those combined nanocomposites demonstrate broadened absorption range, diversity of surface properties, and improved separation of photogenerated charge carriers. The response of magnetic circular dichroism spectroscopy in the CuS near-IR (NIR) spectral region has an inverted sign with respect to that of Au, disclosing that the oscillating charge carriers inducing the surface plasmon behavior in CuS (p-type) and Au (n-type) are of different

Received: February 14, 2023

Revised: April 18, 2023

Published: May 4, 2023



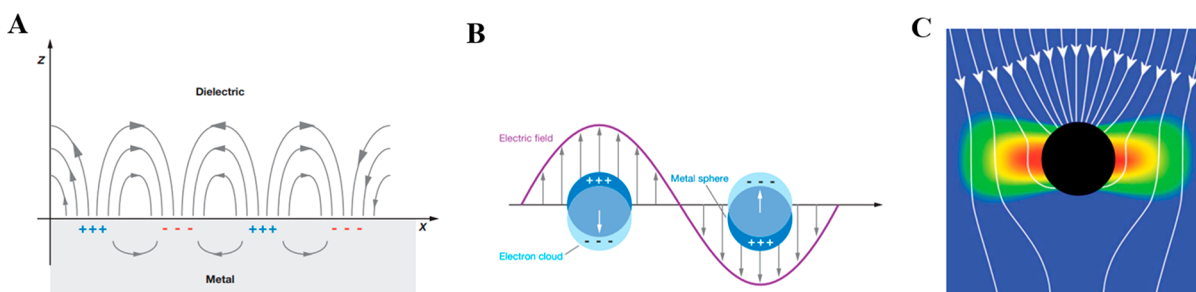


Figure 1. Schematic diagrams illustrating (A) a surface plasmon polariton (or propagating plasmon) and (B) a localized surface plasmon. Reproduced and adapted with permission from ref 25. Copyright 2007 Annual Reviews. (C) The image illustrates the energy flux (Poynting vectors) that neglects scattering effects and the electric field intensity for an incident electromagnetic wave with an electric field in the plane of the image. Red/blue is high/low electric field intensity. Reproduced and adapted with permission from ref 24. Copyright 2012 Royal Society of Chemistry.

natures.¹⁰ The feature of the highest interest is the tunability of the LSPR position in the spectrum, which allows their optimization for potential applications. Because the density of free electrons in metals cannot be easily manipulated, the main method to change the resonance frequency is by varying the nanoparticle morphology. The formation of cation vacancies in the copper chalcogenide counterpart generates free charge carriers, which interact with the electromagnetic field of light and result in a lower energy LSPR mode due to the lower density of free holes ($\sim 2 \times 10^{21} \text{ cm}^{-3}$), compared to free electrons in metallic NPs. When the plasmonic semiconductor is deposited onto a noble metal NP, its LSPR position may be influenced by charge carrier redistribution between the two components, with the free holes diffusing from the vacancy-doped copper chalcogenide to the noble metal and electrons delocalized in the opposite direction.⁸ Adjustment of the free hole concentration in the semiconductor shell is the foundation for the tuning of multiple plasmonic resonance modes present in hybrid nanostructures. In addition, both resonances are affected by the dielectric properties of the complementary component because of higher refractive indexes compared to the surrounding medium. The interaction strength between two plasmons was quantified for Au@Cu_{2-x}S nanostructures based on an anisotropic metallic core.¹¹ The reported coupling strength between the plasmon resonance of the Cu_{2-x}S shells and the longitudinal SPR of the Au nanorod cores was 180 meV, while in the case of transverse LSPR it was found to be only 55 meV because its spectral position is far from the plasmon energy of a semiconductor. Due to the unique electronic properties of heavily doped semiconductors that have tunable plasmonic and excitonic bands,¹² some specially designed noble metals–nonstoichiometric copper chalcogenides nanocomposites may show the plasmon–plasmon interactions as well as plasmon–exciton interactions.^{13–15} Optical properties of such heteronanocomposites are defined by the hybridization of the inner core and the nanoshell plasmons. The coupled dual plasmonic interaction is an energy or charge carrier transfer between two materials and takes less than 100 fs, which is faster than phononic or thermal processes.¹⁶ Dual plasmonic nanostructures exhibit a stronger local electric field enhancement at the interface when both LSPRs are excited compared to the sole excitation of a noble metal or copper chalcogenide, which leads to improved photocatalytic properties.¹⁷ According to numerical calculations, it is possible to tune resonance wavelength and plasmon strength by varying the dimensions of nanostructures.¹⁸ A special type of dual plasmonic

nanostructures are those with harmonically coupled plasmonic resonances when one resonance is energetically located at an excitation energy and the other resonance is located at a harmonic of the excitation frequency. When compared with individual Au and CuS nanoparticles, enhanced second-harmonic light yield by a factor of 3.3 was observed for Au/CuS nanoparticle films.¹⁹ These resonantly coupled plasmonic nanocrystals are promising candidates for the tunable wide-range emission of upconverted light. Moving the CuS or Au LSPR away from the excitation frequency switches the harmonic generation upconversion mechanism to multiphoton photoluminescence.²⁰ Moreover, interparticle plasmon hybridization that depends on separation distance and shell thickness was theoretically demonstrated.²¹ The coupled plasmon resonance modes of neighboring hybrid nanostructures are highly sensitive to the refractive index of the surrounding environment, which can be used as a sensing tool.

We start this review by briefly discussing the localized surface plasmon resonance phenomenon and its energy dependence on the stoichiometry, structural and optical properties of copper chalcogenide NPs. Next, an overview of recently reported synthetic approaches to fabricating noble metal – copper chalcogenide heterostructures with different counterparts' arrangements is presented followed by promising applications of dual plasmonic heteronanocomposites. Lastly, some recommendations for future research directions in the field are listed.

2. LOCALIZED SURFACE PLASMON RESONANCE (LSPR)

Metals, according to the Drude–Lorentz model, can be considered plasma because they contain stationary positive ions and free highly mobile conduction electrons. The free carriers oscillate collectively and coherently in relation to the lattice of positive ions. Such quantized plasma oscillations are referred to as plasmons. However, only surface electrons mainly contribute to the surface plasmon resonance (SPR) because the penetration depth of an electromagnetic wave is around 50 nm.²² Surface plasmons, excited by photons, are electromagnetic excitations propagating at the conductor–dielectric interface and confined in the perpendicular direction. The coupling of the electromagnetic fields to the oscillations of the electrons gives rise to electromagnetic surface waves. These oscillations of the free electron gas in metal and the consequent displacements of electron gas with respect to the fixed ionic cores are caused by the presence of an external

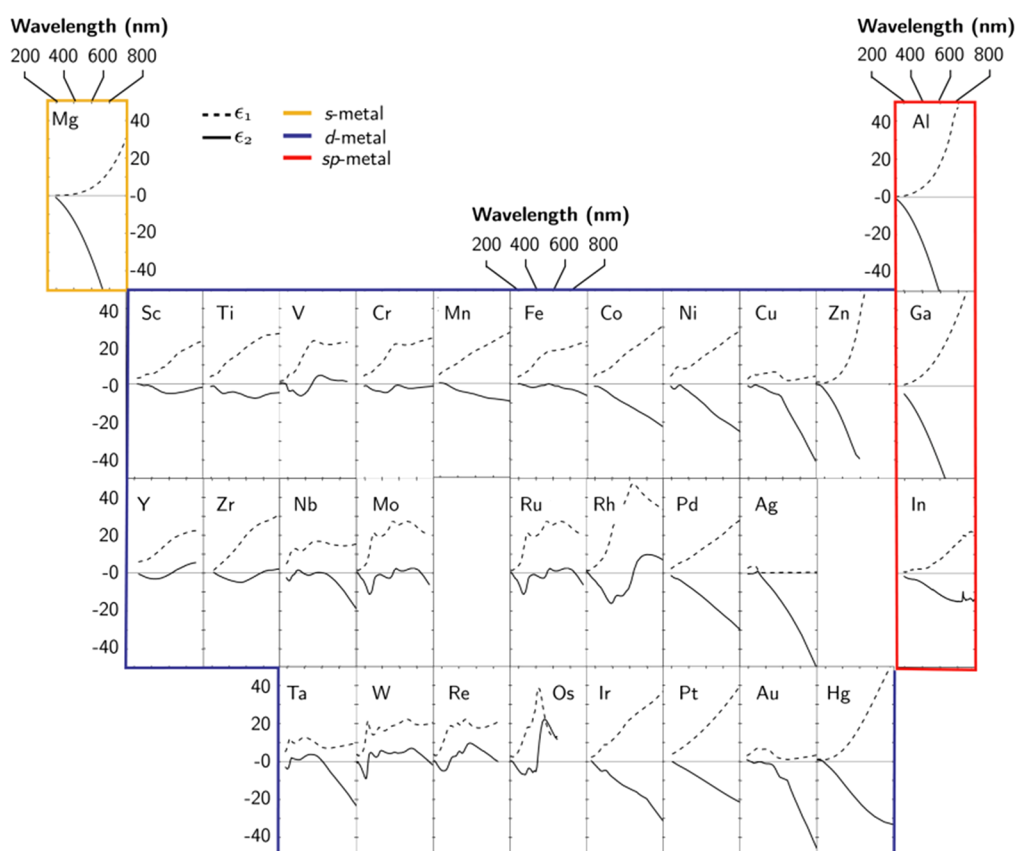


Figure 2. Real (solid line) and imaginary parts (dashed line) of the wavelength-dependent complex dielectric function for different metals. Reproduced with permission from ref 28. Copyright 2020 American Institute of Physics.

electric field. SPR propagates continuously for distances ranging from tens to hundreds of micrometers by prism coupling or grating on a thin metal film surface and is called propagation SPR (PSPR) (Figure 1A). The SPR occurs when the frequency of incident light matches the frequency of oscillating surface electrons. The interaction with photons causes high absorption and scattering cross sections, allowing energy flow within a much larger area than the actual geometric cross section.^{23,24} On the other hand, localized SPR (LSPR) arises when plasmons are confined in a particle of the same or smaller than the wavelength of the incident light (Figure 1B).²⁵ The electron oscillations and the redistributed charge density arouse a local electromagnetic field enhancement near the surface by localizing the incident photons of a certain frequency near its surface (Figure 1C).²⁶ For colloidal noble metal NPs with a diameter of 10–200 nm, the enhancement factor can reach 10,000.²²

Plasmonic materials have been known to our ancestors who used them as pigments for stained glass windows and dyes for textiles. The most famous example is the Lycurgus cup, created by the Romans in 400 A.D., which reflects green light and transmits red light. However, the underlying mechanism for such a color change by the glass object with gold and silver nanoparticles embedded in it was unknown at that time. Nowadays, in addition to Au and Ag, some other metals have been reported to generate surface plasmons, like copper (Cu), aluminum (Al), indium (In), and sodium (Na).^{27,28} The capability to generate surface plasmons is a direct consequence of the material complex dielectric function

$$\varepsilon(\omega) = \varepsilon'(\omega) + i\varepsilon''(\omega)$$

which includes the real part $\varepsilon'(\omega)$ and the imaginary part $\varepsilon''(\omega)$ related to the loss of energy within the medium. The condition of the resonance appearance is a negative real and a small positive imaginary dielectric constant of a material.²⁹ From these considerations, gold (Au) and silver (Ag) support higher quality LSPR than most other plasmonic materials and have been the most investigated materials in plasmonics in the visible and near-infrared (NIR) spectrum (Figure 2).

Both SPR and LSPR are sensitive to the dielectric coefficient (or refractive index, n) of the environment, and it is possible to adjust the resonant frequency by changing the refractive index of the surrounding media. The resonant frequency ω_{LSPR} can be estimated by the following formula:

$$\omega_{LSPR} \approx \frac{\omega_p}{\sqrt{1 + 2\varepsilon_m}}$$

where ε_m is the dielectric constant of the medium ($\varepsilon_m \approx 1.78$ for water at room temperature and $\varepsilon_m \approx 9.00$ for TiO_2) and ω_p is the plasma frequency of the bulky metal as given by

$$\omega_p = \sqrt{\frac{n_e e^2}{\varepsilon_0 m}}$$

where n_e is the density of electrons, e is the electric charge, and m is the effective mass of the electron.³⁰

Besides the electron density n_e and the medium dielectric constant ε_m , the LSPR frequency also depends on shape and particle volume. A copious number of publications have been

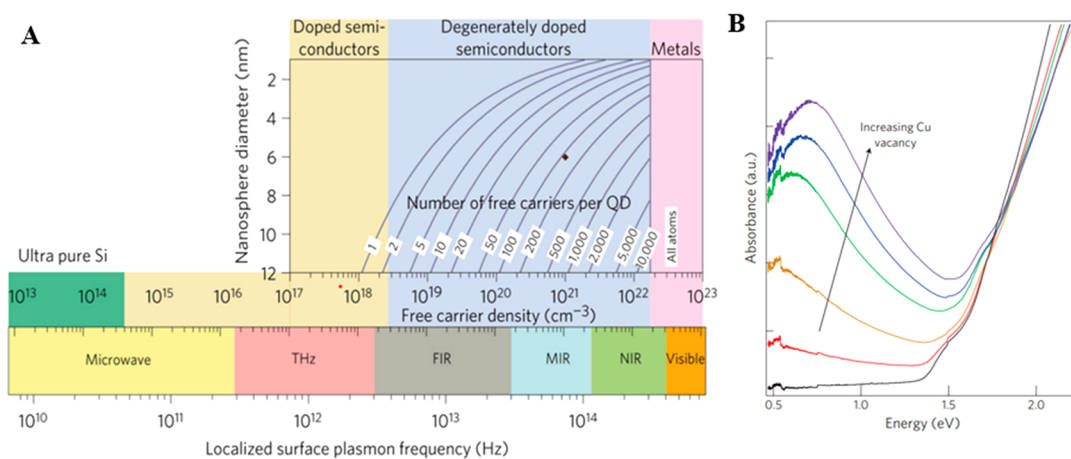


Figure 3. (A) A two-dimensional plot based on the Drude model shows the LSPR frequency as a function of the diameter of the nanocrystal (*y*-axis) and the number of free carriers (contour lines), illustrating the wide range of LSPR frequencies accessible by control of the carrier density of a semiconductor nanocrystal. (B) Cu_{2-x}S nanocrystals display the LSPR that is tunable by control of the vacancy density within the nanocrystal. Reproduced with permission from ref 7. Copyright 2011 Springer Nature.

devoted to the investigation of the ability to change these two parameters in a controllable manner for surface plasmon resonance tuning. Developed approaches to obtain NPs of various shapes, dimensions, solid, and hollow structures open the opportunity to manipulate the resonant wavelengths, optimizing their spectral properties for prospective applications.

As an alternative to metals, several materials including transition metal oxides, nitrides, and chalcogenides have been proposed to be used in plasmonics. Recently, significant attention has been focused on doped copper chalcogenide (Cu_{2-x}E , $\text{E} = \text{S}, \text{Se}, \text{Te}$) nanocrystals for plasmonic applications. Copper chalcogenide NPs show complex stoichiometry-dependent structural and optical properties.³¹ Synthesized Cu_2E NPs are nonstoichiometric, and vacancy doping determines the crystal structure of the product.³² The family of semiconductor Cu_{2-x}E NPs possesses LSPRs positioned in the NIR region, which arise from a high density of free holes induced by copper deficiencies (Figure 3A). The LSPR position is determined by the copper deficiency (x): these binary nanocrystals with the higher x values exhibit intense extinction peaks in the NIR spectrum, while the stoichiometric Cu_2E NPs or slightly cation-deficient with low values of x do not possess a sufficient number of free carriers and plasmonic properties are absent (Figure 3B).⁶ LSPR peak energy increases with the oxidation extent of copper ions, which is a result of the higher number of free holes created. The LSPR properties of copper chalcogenide NPs can be adjusted by changing the size, shape, and complex dielectric function of the material, similarly to metal nanoparticles. For example, rational tuning of the LSPR of anisotropic Cu_{2-x}S NPs has been achieved by obtaining nanoplates of various diameters at a constant thickness of approximately 4 nm.³³ The effect of shape on the LSPR was demonstrated by synthesizing tetragonal phase Cu_{2-x}Te nanorods, nanoplates, and nanocubes.³⁴ An exceptional feature of copper chalcogenide NPs is the possibility to reversibly tune the doping level and the corresponding concentration of charged carriers, shifting the LSPR peak simultaneously. The regulation of the free carrier concentrations has been demonstrated through the nature of the dopant and its concentration, which is not amenable in metal NPs.³⁵ Also, when nonstoichiometric NPs are mixed

with a reducing agent, electrons are transferred to copper chalcogenide bringing the concentration of positively charged carriers down and causing redshift of the LSPR band.³⁶ An alternative approach to adjusting the density of free holes in colloidal copper chalcogenide NPs is *in situ* tuning of LSPR. It has been demonstrated that the density of charge carriers in copper chalcogenides decreased when oleic acid was used as a precursor during synthesis because the deprotonated carboxyl group attached to the surface of synthesized NPs acted as a hole trap.³⁷

3. DUAL PLASMONIC HYBRID NANOARCHITECTURES WITH TUNABLE COMPOSITIONS AND TAILORED PROPERTIES

Due to the structural differences and large lattice mismatches between Au and copper chalcogenides, it remains challenging to directly form well-defined heteronanostructures. We restrict the discussion of dual plasmonic noble metal–copper chalcogenide synthesis to chemical routes in the colloidal state. The majority of core–shell nanoparticles are produced through two main strategies: 1) formation of the core NPs first, followed by coating the core structure with the layer of shell material, and 2) ion exchange reactions.

In the first method, the core acts as a substrate and its surface serves as the nucleation centers offering crystallographic facets for the shell atoms to nucleate and grow. One advantage of the method is its simplicity and possibility to perform reaction in “one pot” by exposing preformed seeds to a supersaturated solution and promoting heterogeneous nucleation and shell deposition. Because the design of multifunctional core–shell nanoparticles depends on their final application, various experimental parameters like the size of seeds, precursors’ concentrations, ratio of seeds to precursors of second materials, stabilization agent, reaction time, and temperature have to be optimized to produce a desired hybrid nanomaterial. The structures of the resulting hybrid nanocomposites are mainly determined by lattice constants of the two materials and the interfacial energy. For uniform deposition of the shell materials on the surface of seeds to obtain traditional concentric core–shell nanoparticles, the lattice parameters of the two materials should be similar and their interfacial energy should be lower than the sum of

their individual surface energies. However, the definition of core–shell nanomaterials has been extended to heterostructures having shell materials partially covering the inner component and can be separately identified. Such eccentric nanohybrids with a reduced common boundary are formed in the systems with high interfacial energy when lattice constant values of two constituents are not comparable or only comparable at a specific facet. The kinetic parameters, such as surfactants, precursor injection rate controlling the diffusion, and shell deposition rate, also affect the shape and function of core–shell structures.³⁸ In the case of large interfacial stress between the shell and the core, self-nucleation and uncontrollable growth of the shell material in the solution separately from dispersed seeds takes place. This restricts the variety of materials that can be incorporated together into hybrid nanoparticles. If incompatibility of the constituents' lattice constants is encountered, an appropriate surfactant or ligand is used for the shell deposition to purposely modify the interfacial energy.

Closed and open topological structures can be achieved by different adsorption strengths of stabilizers on metallic core NPs serving as seeds for heteronucleation.^{14,39} Ligand molecules determine the numbers of reactive sites on the core NPs surface and the topological structures of the produced nanohybrid structure. The shell material has to penetrate through the stabilizer's molecules adsorbed on the surface of core NPs and, eventually, replace them. If the shielding effect of the stabilizer is weak, growing material readily replaces it and occupies all the surface sites of core material forming core–shell nanostructures with the largest interface between them. For example, the influence of polymers and surfactants on the growth mode and the formation of Au–Cu_{2–x}Se was shown.¹⁴ Due to their different adherence to the surface of Au core NPs, heteronanostructures with distinct geometries were formed in the presence of nonionic, anionic, and cationic polymers and surfactants. Tailoring the architecture of such hybrid nanostructures could improve their characteristics, performances, and functions. For instance, the concentric core–shell geometry can maximize the interfacial area and thus provide a platform for studying the plasmon coupling and plasmon–exciton interactions, while asymmetric nanostructures possess different properties, such as charge and polarity, at opposite sides and offer a diversity of active sites for catalysis.

Nanoparticle ion exchange reactions provide a powerful postsynthetic modification technique for designing heteronanostructures while preserving the shape and monodispersity of parental nanocrystals. This fabrication strategy involves a replacement of cations or anions in a nanoparticle with corresponding species in the solution. Ion exchange reactions enrich the library of heterostructures due to the ability to obtain shell material in a metastable phase. The process, which is known for bulk materials to be slow, becomes especially attractive with nanoscale materials as it accelerates greatly due to high specific surface area and low atomic count. Still, the anions have a lower rate of diffusion compared to the cations as well as a larger size requiring elevated temperatures for exchange reaction, which often cause crystal structure and morphology changes producing hollow nanostructures. Therefore, mainly cation exchange reactions that maintain the anion sublattice and undergo topotactic transformation are used to produce the various types of complex nanosystems.⁴⁰ Cation exchange circumvents challenges of a surface-mediated

nucleation approach because prefabricated NPs can be used as anion templates to obtain desired nanocomposites, synthesize hybrids with thermodynamically metastable phases, or tune the direction of the exchange achieving regioselective modification. Full control over the process conditions (i.e., quantity of foreign cation precursor, reaction temperature, or reaction time) along with other parameters, such as the miscibility of reactant and product, determine the outcome of cation exchange to produce homogeneous nanocrystal or favor partial cation exchange forming alloy, doped, or multidomain nanosystem containing the host and the exchanged phases. The reaction finishes spontaneously when the products of a partial cation exchange reach the stable phases and metal cations stop their diffusion.

The architecture of nanomaterials depends on the combination of kinetic and thermodynamic factors.⁴¹ Two phases will arrange in a concentric core–shell if their lattice constants are similar and form sandwiched or Janus heteronanostructure minimizing the heterointerface area for materials with a large lattice mismatch. The thermodynamics of a cation exchange reaction is determined by the difference in formation energies of the reactant and product phases and the difference in redox potentials of the exchanging ions. However, the formation energies could change at the nanoscale and, since surface energy has a dominant contribution to the lattice energy, may depend on crystallite size and shape as well as contribution from the capping agent. The high surface area of nanocrystals lowers the reaction activation barrier that together with other factors, like an excess of the incoming cations and favored solvation of the host lattice cations, carries the reaction at room temperatures. Once an original NP is exposed to a solution containing exchange cations, the inward and outward diffusion fluxes start through defects, a vacancy-assisted or an interstitial mechanism. A driving force for such directional diffusion is a chemical potential gradient within nanomaterial due to the difference in surface and inner NP part compositions. The cation exchange process is kinetically limited by the rate of solid-state diffusion.

Transformations between the first and second group cation chalcogenides via cation exchange reactions can be used to convert metal chalcogenide shell (e.g., Ag₂S, CdS) into nonstoichiometric copper chalcogenide in complex heteronanostructures.⁴² This synthetic approach provides precise control of the final Cu_{2–x}S phase.⁴³ At short reaction times and low precursor concentrations, the Cu_{2–x}S forms in a roxbyite phase. However, with an increased reaction time and amount of the precursor, the djurleite Cu_{2–x}S structure appeared.

We provide the summary of recently reported synthetic methods, specifying precursors and reaction conditions, used to form dual plasmonic noble metal–copper chalcogenide nanocomposites of desired structural arrangement in Table 1 and elaborate them further in following subsections.

3.1. Dual Plasmonic NPs Based on Isotropic Core. Due to the strong coupling of metallic and nonmetallic plasmons, dual plasmonic hybrid nanocomposites display excellent plasmonic extinction and enhanced photocatalytic and photothermal properties. One of the factors that influence the properties of such dual plasmonic heteronanostructures is the concentration of copper vacancies in the semiconductor shell. Tunability of copper chalcogenide shell stoichiometries and control of its crystalline phases is challenging. Wang et al. synthesized Au@Cu_{2–x}S core–shell nanostructures with well-controlled dimensions and free hole concentration in the shell

Table 1. Overview of the Experimental Procedures for the Synthesis of dual plasmonic noble metal–copper chalcogenide hetero-nanostructures

Heterostructure Type	Chemical Notation	Chemical Approach	Chalcogenide Precursor	Cu-Precursor	Reaction Conditions	References
Concentric	Au@Cu _{2-x} S	seed-mediated growth	Spherical Metallic Core–Solid Copper Chalcogenide Shell Thioacetamide N,N-dimethyl-selenourea	CuSO ₄ ·5H ₂ O	PVP, sodium citrate, NaOH (to pH ~ 9.3), hydroxylamine hydrochloride, at 70 °C under the N ₂ for 10–12 h	4, 10, 56
	Ag@CuS	seed-mediated growth with postsynthesis phase transitions	thiourea	Cu(NO ₃) ₂	ethylene glycol, PVP, at 197 °C for 10–40 min, H ₂ O ₂	44
	Au@Cu _{2-x} Se	seed-mediated growth with postsynthesis phase transitions	sulfur in 1,2-dichlorobenzene	Copper(II) acetylacetonate	oleylamine, at 100 °C for 30 min, under the N ₂	45
	Au@Cu _{2-x} S	hydrothermal method	thioacetamide	Cu(NO ₃) ₂	CTAB, AA, hexamethylenetetramine, at 80–90 °C for 4.5–8 h in a vacuum oven	47, 90
	Au@Cu _{2-x} Se	selenium-mediated with Au@Se formation	SeO ₂	CuSO ₄	PVP, AA, at 30 °C for 10 h	53, 54
Eccentric	Au/CuS	seed-mediated growth	sulfur in 1,2-dichlorobenzene	Copper(II) acetylacetonate	oleylamine, at 100 °C under Ar atmosphere for 30 min	16, 46
	Au–CuS	selenium-mediated with Au@Se formation	SeO ₂	CuSO ₄	CTAC, AA, at room temperature for 40 min-overnight	9, 17
Core–Shell to Dimer	Au@Cu _{2-x} S	phase segregation of AuCu alloy	thioacetamide selenourea	Cu(NO ₃) ₂	PVP, tetraethylene glycol, at 200–280 °C for 15 min	50
	Au@Cu _{2-x} Se	tellurium-mediated with Au(0)-Te formation	Te powder in dodecanethiol	CuCl ₃ in octadecylamine	at 180 °C, under N ₂ for 10 min	55
	Au/Cu _{2-x} S NRs	hydrothermal method	Anisotropic Metallic Core–Solid Copper Chalcogenide Shell thioacetamide	CuCl ₃ Cu(NO ₃) ₂	CTAB, AA, hexamethylenetetramine, at 85–90 °C for 4.5–8 h in a vacuum oven	11, 47
Disk-on-Dot	Au NRs–Cu _{2-x} S ₄	hydrothermal method with a site-selective growth	(PhCOS) ₂ Ni	Cu(NO ₃) ₂	NaOH (to pH ~ 9), at 140 °C for 2 h in a Teflon-lined stainless-steel autoclave	60
	Au NRs–Cu _{2-x} S	heterogeneous nucleation and growth with a “reactive site regulation” strategy	bovine serum albumin	CuSO ₄ ·5H ₂ O	CTAB, NaOH (to pH ~ 12), undisturbed 6 h in 80 °C water bath	39
	Au@Cu _{2-x} S NRs	cation exchange	sulfur powder mixed with Na ₂ S·9H ₂ O	Cu(CH ₃ CN) ₄ PF ₆ in methanol	CTAB, AgNO ₃ , AA, NaOH, Cd(NO ₃) ₂ ·4H ₂ O in methanol, tributylphosphine, ethylene glycol	88
Elongated Exotic Structures	Au@(Cu _{2-x} S–Ag ₂ S)	hydrothermal method using incompletely coated Au/Ag ₂ S heterostructure	thioacetamide	CuCl ₃	CTAB, AA, hexamethylenetetramine, pH ~ 5.0, at 85 °C for 2–8 h in an oven	13, 59
	Au@(Cu _{2-x} S–Cds)	Se template method	SeO ₂	Cu(NO ₃) ₂ ·3H ₂ O	CTAB/CTAC/PVP/PSS/PDDA, AA, at room temperature for 40 min-overnight	63, 66
Hierarchical Structures	Au@Cu _{2-x} S	the Kirkendall process with anion exchange using Au@Cu ₂ O template	Metallic Core–Hollow Copper Chalcogenide Shell Na ₂ S thioacetamide 1,1-dimethyl-2-selenourea	CuCl ₃	PVP, NaOH, hydrazine, at 75 °C for 2 h	70
	Au–CuS	site-selective heterogeneous nucleation	Copper Chalcogenide Core–Metallic Shell sulfur powder in oleylamine	CuCl ₃	toluene, oleylamine, oxalic acid dihydrate in methanol, HAuCl ₄ ·3H ₂ O in methanol, for 5 min in a nitrogen-filled glovebox at room temperature and under exclusion of light	78
Satellite Structures	Cu _{2-x} Se–Au	heterogeneous nucleation	Na ₂ SeO ₃ , SeO ₂	CuSO ₄ ·5H ₂ O	bovine serum albumin, AA, HAuCl ₄ , at room temperature for 3 h	86, 87

Table 1. continued

Heterostructure Type	Chemical Notation	Chemical Approach	Chalcogenide Precursor	Cu-Precursor	Reaction Conditions	References
	CuS–Au	galvanic exchange	(NH ₄) ₂ S	CuCl ₂ ·2H ₂ O	PVP, HAuCl ₄ ·4H ₂ O, at room temperature for 0.5–5 h	80
	CuS@Au	cation exchange and redox reactions between CuS and Au ³⁺ ions	sulfur in octadecene and oleylamine	copper(II) acetate monohydrate	HAuCl ₄ ·3H ₂ O in methanol, AA in methanol, at room temperature in a N ₂ -filled glovebox for 0.5–24 h	75
Hollow Core–Dotted/Spiky/Islanded Shell	Au/CuS	heterogeneous nucleation with tunable surface topography	Na ₂ S	copper(II) acetate	HAuCl ₄ , AA, at room temperature for 30 min	77
	CuS@Au					

deposited on a prefabricated core.⁴⁴ The researchers selectively grew copper sulfide nanoshells with targeted crystalline phases, like covellite (CuS), digenite (Cu_{1.8}S), and nonstoichiometric Cu_{2–x}S (Figure 4A–F). They used Cu(NO₃)₂ and thiourea as the Cu and S precursors in ethylene glycol for this colloidal phase-selective synthesis at high temperatures. To obtain Cu-deficient covellite or Cu-rich digenite as well as control of the shell thickness, different molar ratios of the Cu and S precursors were added. Furthermore, the digenite phase shells could be converted into nonstoichiometric Cu_{2–x}S by a mild oxidizing agent, like H₂O₂, increasing the concentration of free holes. Consequently, Au NPs coated with different copper sulfide phases show distinctive spectral features. In the optical extinction spectra of colloidal Au@covellite core–shell nanostructures, three different bands appeared, corresponding to plasmon resonance of copper sulfide hot holes, gold hot electrons' oscillations, and the interband electronic transitions from the valence (VB) to the conduction (CB) band of CuS with an increase of energy (Figure 4A). Au@Cu_{1.8}S nanostructures exhibit only two peaks correlating with plasmonic electron oscillations of the Au cores and the VB-to-CB transitions in the shell (Figure 4C). Due to the very low density of free holes in Cu_{1.8}S, extinction spectral features associated with the semiconductor plasmons are positioned far beyond the observed spectral range. However, after the treatment with H₂O₂, the digenite shells were converted into nonstoichiometric Cu_{2–x}S phases. Because the number of Cu vacancies gradually increased, a broad extinction peak emerged in the NIR region, progressively intensified, and blue-shifted with time (Figure 4E). Together with optical properties, morphological characteristics of dual plasmonic gold–copper selenide hybrids changed. When multicrystalline CuS shells grew on the Au core, flower-like nanocomposites were formed, because of the intrinsic structural anisotropy of covellite (Figure 4B). While after the digenite deposition heretofore nanostructures possessed a spherically symmetric core–shell structure due to the cubic phase of the shell and small lattice mismatch between core and shell (Figure 4D). After the treatment of the Cu_{1.8}S shell with H₂O₂, it was transformed into a loosely packed nonstoichiometric Cu_{2–x}S phase, which preserved the morphology of the original heteronanostructures (Figure 4G).

Several other synthetic approaches were developed to form Au@Cu_{2–x}S nanohybrids with a spherical core. To synthesize the plasmonic Au–Cu₉S₅ core–shell and Au–CuS hybrid dimer nanocrystals by solvothermal method, dissolved elemental sulfur was added in the dichlorobenzene, containing Au seeds and copper(II) acetylacetonate in the presence of oleylamine as a surfactant at 80 °C under an inert atmosphere of N₂.^{45,46} Also, synthesis of Au/Cu_{2–x}S hybrids was performed in aqueous-based solutions using thioacetamide as a source of sulfur at the elevated temperature (90 °C) in a vacuum oven for 4.5 h.⁴⁷ Moreover, kinetic control of reaction conditions, specifically time, permitted the formation of defined Janus or core–shell nanostructures while all other conditions were kept the same.

One more robust and versatile colloidal synthetic approach for the synthesis of dual plasmonic Au@copper chalcogenide heteronanostructures is through the formation of an Au–Cu alloy nanoparticle and then induction of phase segregation to form a two-component product.^{48–50} Because a binary Au–Cu alloy system forms stable intermetallic compounds with a variety of atomic ratios, the composition of the produced

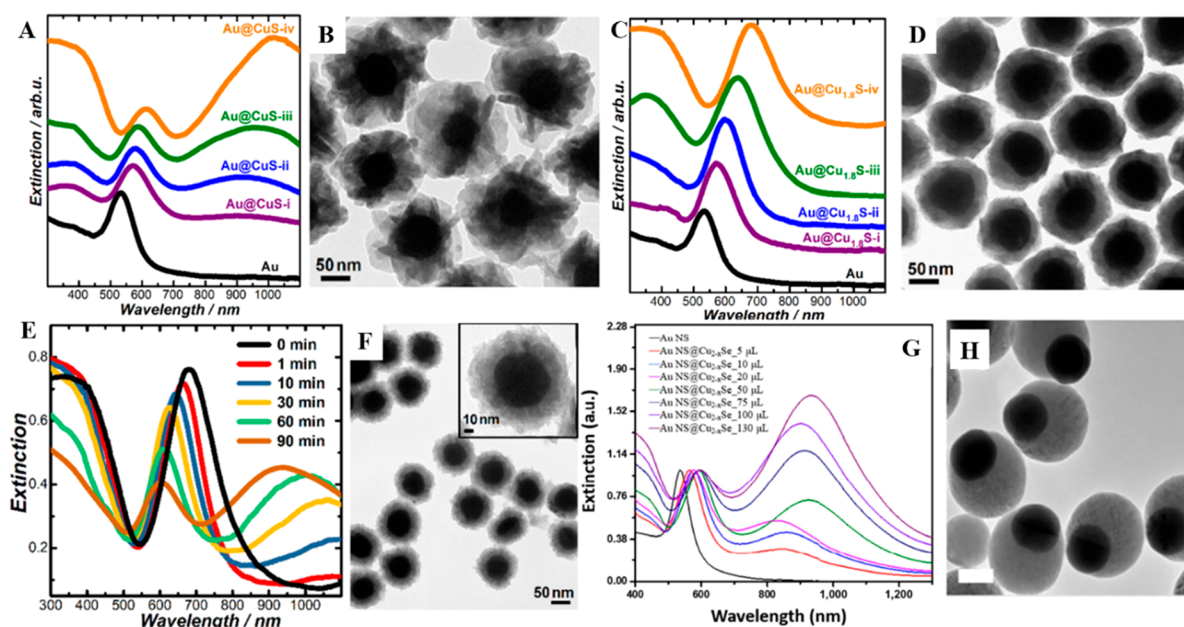


Figure 4. (A) Optical extinction spectra of colloidal Au NPs, Au@CuS core–shell NPs with increasing CuS shell thickness. (B) TEM images of Au@CuS core–shell NPs composed of 62 nm Au cores and the thickest CuS shell. (C) Optical extinction spectra of colloidal Au NPs and Au@Cu_{1.8}S core–shell NPs with increasing Cu_{1.8}S shell thickness. (D) TEM images of Au@Cu_{1.8}S core–shell NPs composed of 62 nm Au cores and thickest Cu_{1.8}S shell. (E) Snapshot extinction spectra of colloidal Au@Cu_{1.8}S core–shell NPs upon exposure to 0.3 mM H₂O₂ at various reaction times. (F) TEM images of the NPs obtained after exposing Au@Cu_{1.8}S core–shell NPs to 0.3 mM H₂O₂ for 90 min. Reproduced and adapted with permission from ref 44. Copyright 2020 American Chemistry Society. (G) UV–vis–NIR extinction spectra of aqueous solutions of Au and eccentric Au@Cu_{2-x}Se nanoparticles with tuned shell thickness. (H) TEM image of eccentric Au@Cu_{2-x}Se nanostructures with Cu_{2-x}Se shell obtained using 75 μ L of 0.01 mol/L SeO₂ during synthesis. Reproduced and adapted with permission from ref 17. Copyright 2021 Springer Nature.

heteronanostructures is predetermined by the concentrations of components in starting Au–Cu nanoparticles. After the conversion of the alloy NPs, the Au core and the copper chalcogenide shell remain adjoined circumventing lattice mismatch issues often encountered during heterogeneous nucleation. Among other advantages of this synthetic approach is a one-pot process of the Au–Cu alloy transformation into dual plasmonic nanocomposites avoiding multistep fabrication. Hybrid Au–Cu₂S nanoparticles were formed in the reaction between colloidal Au–Cu nanoparticles with sulfur dissolved in oleylamine while bubbling oxygen to activate the reaction by forming some intermediate on the surface.⁴⁸ Alternatively, this protocol was simplified by using 1-dodecanethiol as a surfactant as well as the sulfur source.⁴⁹ Recently, this method was used to obtain not only Au–Cu₂S NPs but also hybrid nanostructures with other copper chalcogenides like Au–Cu₂Se.⁵⁰ The researchers were able to manipulate architectures of the final structures, tune domain sizes, and obtain desired crystalline phases. To control the crystalline phases of the copper chalcogenide domains, the concentration of chalcogen precursor and the reaction temperature had to be modified. The chalcogenization step promoted the diffusion of Au and Cu atoms in the alloy and required higher chalcogen precursor concentrations for Au-rich alloy NPs due to decreased atomic mobilities. The rate of Cu diffusion must be slower than the reaction with chalcogen for the Au and copper chalcogenide to remain adjoined to ensure the nucleation of the shell material takes place near the nanoparticle surface. To guarantee the complete transformation to copper chalcogenide, reaction temperature was raised higher for Cu-rich digenite and berzelianite phases.

The dissimilarity of crystalline structures, such as atomically disordered alloy phases and ordered intermetallic structures at

the nanoscale exhibit distinct behaviors toward the morphologies of the dual plasmonic hybrid heteronanostructures. For the chemically triggered phase separation method with intermixed bimetallic Au–Cu nanoparticles as the starting materials, the formation of atomically ordered intermetallic phases effectively suppressed the ion diffusion of chalcogenide precursors due to the higher energy barriers, restricting the atomic exchange and migration exclusively at the interfaces in comparison to the disordered alloy structures. Hence, the structure-transforming kinetics are different than those of less stable atomically disordered alloy structures. To be exact, the sulfidation and selenidation of intermetallic nanoparticles were significantly slower than that of alloy phases. The phase segregation of the intermetallic nanoparticles occurred more slowly than that of their alloy counterparts, and the metallic domains gradually became smaller in size as Cu atoms diffused into the growing copper chalcogenide domains. However, the phase transition was almost independent of the atomic ordering or the Cu/Au stoichiometries but primarily determined by the chalcogen precursor concentrations as well as the reaction temperatures. During the process of the nanoscale Kirkendall effect, the nonequivalent diffusion rates of two different ions caused the interface to migrate toward one direction while forming voids and cavities at the boundaries of the materials, and the diffusivity of ions or velocity at which the boundary interface moves can be quantitatively described in the Darken's equation. The kinetics of atomic diffusion was not only influenced by the structural stoichiometries but also by the ordering of Au and Cu atoms. The atomic diffusion rates at the same Au/Cu stoichiometric ratios in the intermetallic particles went slower than those in the alloy particles, and such a difference in diffusivities led to remarkably different

transforming behaviors of both alloy and intermetallic particles during the synthesis of dual plasmonic nanostructures.

Adjusting the Cu/Au stoichiometries of the template bimetallic nanoparticles, the shell dimensions could be varied in the final hybrid nanostructures. Moreover, distinct copper chalcogenide morphologies were observed: CuS formed a spiky shell, while CuSe grew in large nanosheets. Control over the shell thickness could be critical for the properties of such nanocomposites. When magneto-optical properties of dual plasmonic NPs were studied, a thicker shell demonstrated higher activity in the NIR region compared to a thin and nonuniform shell.¹⁰ Additionally, it was shown that coating dual plasmonic hybrid nanostructures with a layer of gold and formation of Au@Cu_{2-x}S@Au NPs results in suppression of the NIR LSPR of the Cu_{2-x}S nanoshell.⁵¹

Previously, for the deposition of a copper selenide shell on an Au core, selenium powder dissolved in oleic acid was used as a selenium precursor and synthesis was performed in organic solvents at a high temperature for prolonged reaction times.⁵² Nowadays, Se template-mediated two-step synthesis is widely used and copper selenide could be coated in aqueous solutions at room temperature. A cubic berzelianite Cu_{2-x}Se shell could form concentric and eccentric Au@Cu_{2-x}Se heteronanostructures in the presence of poly(vinylpyrrolidone) (PVP)^{53,54} or hexadecyltrimethylammonium chloride (CTAC), respectively.¹⁷ At first, the Se shell was deposited onto the Au core, and then Cu²⁺ ions were added to the solution of Au@Se intermediates containing ascorbic acid and reduced to monovalent Cu⁺ before being incorporated into the Se sublattice to form copper-deficient Cu_{2-x}Se upon the exposure to air. The preferential growth of Se on one side of uniform Au NPs could be explained by the relatively strong blocking of the Au NPs surface sites by CTAC, which facilitates the deposition of subsequent layers of growth material on previously nucleated Se (Figure 4H). The overgrowth of selenium to form an interfacial bridging layer depends critically upon the absorption strength of capping ligands or stabilizers on the noble metal seeds. Normally, a strongly absorbing stabilizer inhibits isotropic overgrowth, which is substantiated by the molecular dynamics simulations. In general, when the shielding effect of capping ligands due to the steric hindrance is quite weak, the growth material can easily penetrate, replace the originally adsorbed stabilizers, and nucleate on the entire seed surface, leading to a concentric and uniform coverage or symmetric core-shell structure via continuous growth, such as poly(acrylic acid) on citrate-coated Au. When the shielding effect is quite strong, the growth materials must nucleate either homogeneously in an aqueous solution or directly on stabilizers, asymmetric heterodimer structures are favored thermodynamically, such as poly(dimethyldiallylammonium chloride) (PDDA) surfactants on the Au surface. In the case of intermediate shielding strength, the nucleation only takes a very limited number of exposed surface sites of Au particles, resulting in eccentric or crescent nanostructures partially encapsulating Au with capping agents of CTAC or hexadecyltrimethylammonium bromide (CTAB) bearing the hydrophilic morphology-directing quaternary ammonium groups. During the subsequent chemical transformation into copper chalcogenides, the final morphology inherited the initial morphology of preformed Au-Se hybrid particles. The final structures of the dual plasmonic nanoparticles are dictated more by the thermodynamic factors for the selenium-mediated multistep strategy.

This method permits the control of the shell thickness by the addition of various amounts of selenium precursor SeO₂ during the synthesis. In extinction spectra of dual plasmonic Au@Cu_{2-x}Se, the plasmonic bands of Cu_{2-x}Se centered at around 900 nm became more pronounced with an increase of shell thickness due to the larger extinction cross section (Figure 4G). The lower degree of copper deficiency in the larger semiconductor shells corresponds to plasmonic resonances of lower energy and results in the redshift of Cu_{2-x}Se LSPRs.

A similar two-step strategy was used to obtain Au-Cu_{2-x}Te disk-on-dot heterostructures,⁵⁵ where Au particles dispersed in oleylamine were used as seeds and Te shell was coated after the addition of Te in thiol as the telluride precursor under a N₂ atmosphere. Then, Cu(II) chloride in an amine medium, reduced to Cu (I), was utilized as the copper source in this synthesis performed at 180 °C. Integration of Au and Cu_{2-x}Te in one heterostructure that shows dual plasmonic properties successfully reduces charge recombination and enhances the photoelectrocatalytic water splitting.

Dual plasmonic heteronanostructures based on an Au core are the most common and actively investigated. However, despite remarkable successes, though few reports devoted to Ag-based dual plasmonic nanomaterials have been published.⁵⁶ Incorporation of an Ag core is highly desired because the higher enhancement of the electromagnetic field is achieved by the stronger interaction of the conduction electrons oscillations within Ag nanoparticles than in gold NPs.⁵⁷ Their disadvantage compared to Au NPs, in the scope of the formation of dual plasmonic heterostructures, is high reactivity. The Ag@CuS core-shell NPs were prepared by a two-step, self-assembly based, and controlled aqueous synthetic method.⁵⁶ PVP-capped Ag NPs were mixed with thioacetamide and CuSO₄ solutions at 70 °C for 10 h in a nitrogen environment. The addition of various reagent concentrations resulted in different shell layer thicknesses. Produced Ag@CuS NPs possess dual plasmonic properties and exhibit corresponding extinction peaks at 400 and 975 nm in the spectrum.

3.2. Regioselective Overgrowth of Copper Chalcogenides on Anisotropic Metal Cores. Anisotropic gold nanoparticles have attracted the interest of scientists because they have different structural, optical, electronic, magnetic, and catalytic properties from those of isotropic structures.

Combining anisotropic Au NPs with copper chalcogenides provides the ability to selectively control the LSPR of each constituent. The seed-mediated growth has become the most efficient and widely used synthetic method of Au NPs of targeted geometries.⁵⁸ Among anisotropic NPs, Au nanorods have been actively studied as a core for dual plasmonic heteronanostructures. The main reason for the nanorod (NR) shape to become a model system is that plasmon resonance in Au NRs can be precisely tuned by controlling their aspect ratio.

Synthetic approaches employed for the fabrication of dual plasmonic gold-nonstoichiometric copper chalcogenide hybrids based on the anisotropic core are similar to those used for heteronanostructures based on the spherical core. Thioacetamide as a source of sulfur for the production of Au@Cu_{2-x}S was usually used at elevated temperatures and prolonged reaction times.^{11,47,59} Another S-precursor reported for the synthesis of Au@Cu_{2-x}S via a hydrothermal reaction was nickel thiobenzoate.⁶⁰ One more strategy for obtaining Au@Cu_{2-x}S is by ionic exchange. For example, Zhang et al.

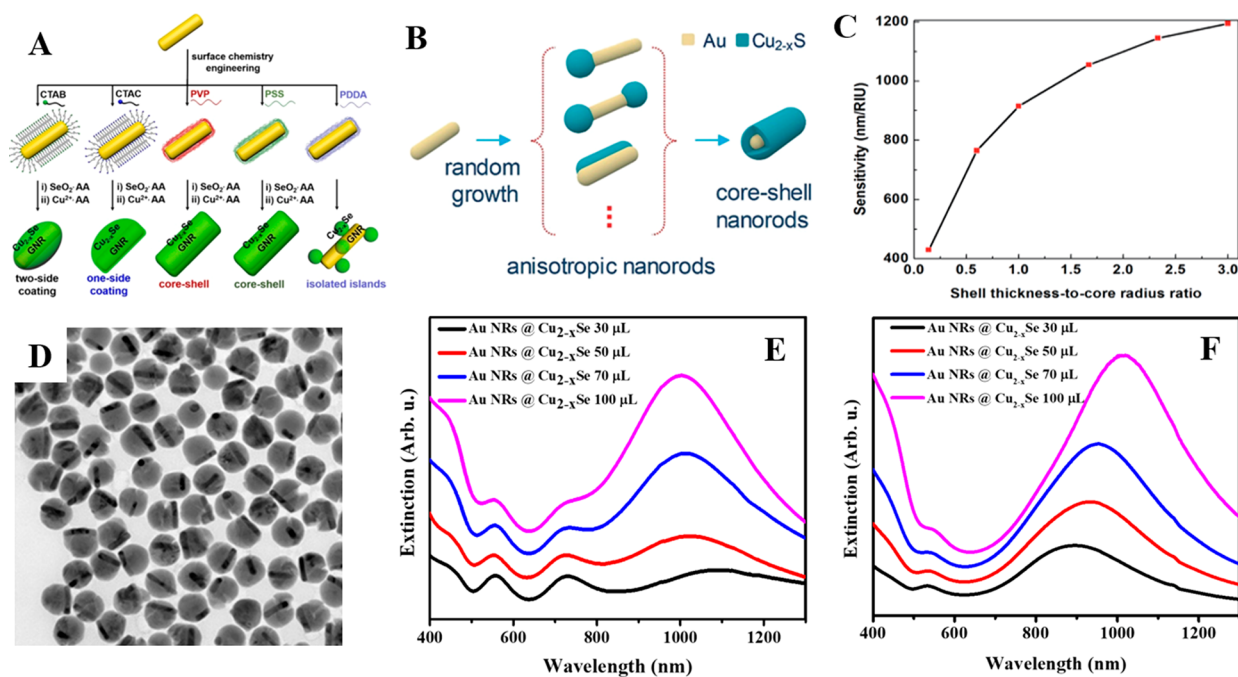


Figure 5. (A) Scheme showing capping agent-mediated overgrowth of Cu_{2-x}Se on the Au NRs for the synthesis of Au NRs@ Cu_{2-x}Se heterostructures via a Se template method. Reproduced and adapted with permission from ref 63. Copyright 2020 Ivyspring. (B) Schematic illustration of the growth behavior of Cu_{2-x}S on Au nanorods. Reproduced and adapted with permission from ref 47. Copyright 2019 The Royal Society of Chemistry. (C) Refractive index sensitivity of Au@ Cu_{2-x}S core-shell NRs with different shell thickness-to-core radius ratios. Reproduced and adapted with permission from ref 65. Copyright 2018 Royal Society of Chemistry. (D) TEM images of Au NRs-2@ Cu_{2-x}Se nanostructures with Cu_{2-x}Se shell size were obtained using 100 μL of 0.01 M SeO_2 in the presence of CTAC. The scale bar corresponds to 200 nm. Extinction spectra of aqueous solutions of Au NRs@ Cu_{2-x}Se nanoparticles with (E) Au NRs-1 with an aspect ratio of 2.4 or (F) Au NRs-2 with an aspect ratio of 3.8. Corresponding volumes of 0.01 M SeO_2 used for synthesis are noted in the figure. Reproduced and adapted with permission from ref 66. Copyright 2022 Royal Society of Chemistry.

elaborated multistep synthesis, which includes the deposition of an Ag shell on Au NRs, its conversion to amorphous Ag_2S , and then to CdS shell that finally was transformed to Cu_{2-x}S by the cation exchange between Cu^+ and the CdS shell.⁶¹ However, the first two steps of obtaining Au@Ag and Au@ Ag_2S intermediates could be omitted.⁶²

To deposit a Cu_{2-x}Se core on Au NRs, the same Au@Se intermediates with amorphous Se and subsequent conversion into nonstoichiometric copper selenide in aqueous solutions at ambient conditions was performed.^{63,64} The shell thickness was successfully adjusted by the addition of various concentrations of SeO_2 during synthesis. The geometry of obtained nanostructures, lateral one- and two-side deposition, core-shell coating, or island growth of copper chalcogenides on the Au NRs could be manipulated using different capping agents⁶³ (Figure 5A) or varying their concentrations in the reaction mixture.³⁹ Coating of Cu_{2-x}Se on the Au NRs in the presence of CTAC resulted in one lateral side overgrowth (Figure 5D) and with a CTAB Cu_{2-x}Se shell was deposited onto both lateral sides. To obtain the complete core-shell heterostructures, PVP and poly(sodium 4-styrenesulfonate) (PSS) could be used. On the contrary, the island growth mode was stimulated by the PDDA stabilizer. A modified synthetic strategy was suggested for precise control of the sites on Au NRs surface where copper sulfide was deposited.⁵⁹ By growing Ag_2S on the Au NRs first, the Cu_{2-x}S shells had limited gold sites available and were forced to grow on the uncovered side surface. The study of the copper sulfide growth on Au NRs revealed several stages, such as initial heteronucleation at random sites of the core surface, formation

of anisotropic nanorods, and enlargement to the core-shell structures (Figure 5B).⁴⁷ This suggests that reaction time could be another factor determining the morphology of the products. Optimization of the shell domain may be critical for certain applications. The effects of the shell-thickness to core-radius ratio have been shown to have more influence on the refractive index sensitivity than the aspect ratio of Au NRs (Figure 5C).⁶⁵

The spectral response of the Au NRs shows the appearance of the transverse and longitudinal surface plasmon resonance bands. After the deposition of copper chalcogenide, in addition to the two resonance peaks of the Au NRs core, one more intense and broader band in the NIR region appeared. The coupling strength between the counterparts of anisotropic dual plasmonic nanocomposites can be modulated by the wavelength gap between the longitudinal LSPRs of the Au NRs core and LSPR of the copper chalcogenide shell.⁶⁶ The effect of the band overlap in anisotropic structures was studied by synthesizing Au NRs cores with different aspect ratios to obtain Au NRs-1@ Cu_{2-x}Se with partial band overlap and Au NRs-2@ Cu_{2-x}Se with a full overlap of plasmonic peaks in the spectrum (Figure 5E,F). Through an elaborate synthesis of the Au NRs core and adjustment of the stoichiometry of the Cu_{2-x}Se shell by the time of oxidation on air and overall shell thickness, the LSPRs of both could be accurately tuned to the same wavelength, and only two LSPR peaks observed in spectra of Au NR-2@ Cu_{2-x}Se colloid. The experiment showed that strong plasmonic coupling between LSPRs of Au and Cu_{2-x}Se is one of the effects contributing to photocatalytic activity, together with a surface area of nanocomposites.

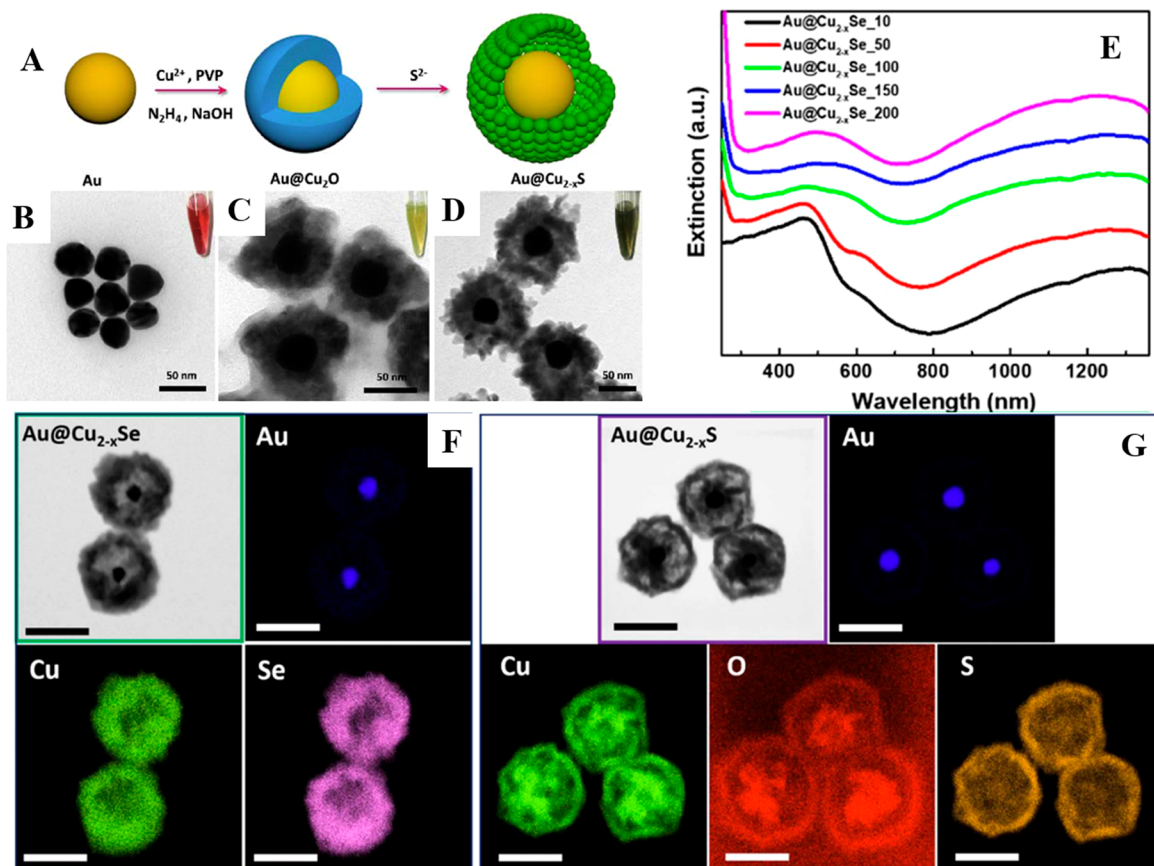


Figure 6. (A) Scheme illustration of the synthesis process of the Au@Cu_{2-x}S hollow mesoporous spheres; TEM images of (B) Au NPs, (C) Au@Cu₂O core–shell NPs, and (D) Au@Cu_{2-x}S hollow mesoporous spheres. Inset: photographs of Au NPs, Au@Cu₂O, and Au@Cu_{2-x}S solutions. Reproduced and adapted with permission from ref 70. Copyright 2017 Elsevier. (E) Extinction spectra of aqueous solutions of hollow Au@Cu_{2-x}Se NPs obtained using 10, 50, 100, 150, and 200 mL of 50 mM 1,1-dimethyl-2-selenourea for synthesis. (F) Elemental distributions of Au, Cu, and Se in hollow dual plasmonic Au@Cu_{2-x}Se. (G) Mapping images of Au, Cu, O, and S in hollow dual plasmonic Au@Cu_{2-x}S. Scale bar: 200 nm. Reproduced and adapted with permission from ref 74. Copyright 2023 Royal Society of Chemistry.

3.3. Dual Plasmonic NPs with Hollowed Shell. Among others dual plasmonic hybrids, hollow noble metal–vacancy-doped copper chalcogenide nanosystems are particularly interesting owing to their unique properties, such as large surface areas, high pore volumes, reduced charge recombination, low densities, accelerated mass transfer, and enriched active sites for adsorption and photocatalysis.⁶⁷ The encapsulation of plasmonic noble metal NPs with isotropic or anisotropic shapes into various hollow nonstoichiometric copper chalcogenides enables the incident light to be reflected multiple times between cores and the shell utilizing the full spectrum of light energy and producing an intense local electromagnetic field enhancement within the nanoparticle.⁶⁸

The most effective approach in the production of hollow dual plasmonic hybrids is the hard template method based on Au@Cu₂O core@shell nanoparticles (Figure 6A). When utilizing the methods based on multistep ion exchange reactions to form dual plasmonic hybrid nanostructures, two key factors are to be considered, including the precise control of the architectural arrangement and the compositional stoichiometries that could synergistically and kinetically maneuver the relative rates of intertwining structure-transforming pathways, such as the nanoscale interdiffusion-mediated Kirkendall effect and thermodynamically driven domain coarsening also referred to as Oswald ripening. To obtain templates with concentric symmetry, PVP is added to

serve as a stabilizer and an agent determining the structure.⁶⁹ Then, Cu₂O shells are converted into a desired copper chalcogenide when a sulfur or selenium precursor is introduced (Figure 6B–D).⁷⁰ Chalcogenide anions react with the copper on the surface of the NCs, diffusing inside the shell simultaneously, while oxygen anions move out. Because of the difference in diffusion rates between anions and cations and the size of anions, the process produces hollow nanostructures. The reaction is spontaneous because the solubility product constants of copper chalcogenides are smaller than that of Cu₂O. Nanostructures maintain the original shape after the transformation of intermediates, but overall dimensions are slightly expanded.⁷¹ This method could be modified by the addition of HCl to remove the inner residual Cu₂O if necessary.⁷²

Compared with the core–shell nanostructures, the hollow systems preserve the fascinating plasmonic effect of the Au core. While the plasmonic response of the Au core is redshifted in the spectrum of the intermediates due to the high refractive index of copper(I) oxide, the LSPR peak corresponding to the Au core returns to its original position in the spectrum of hollow dual plasmonic nanostructures, which also demonstrates an enhanced absorption in the NIR region (Figure 6E).⁶⁹ Hence, the position of the Au plasmon resonance peak was unaffected by the high refractive index of the copper chalcogenide shell due to the gap between the two

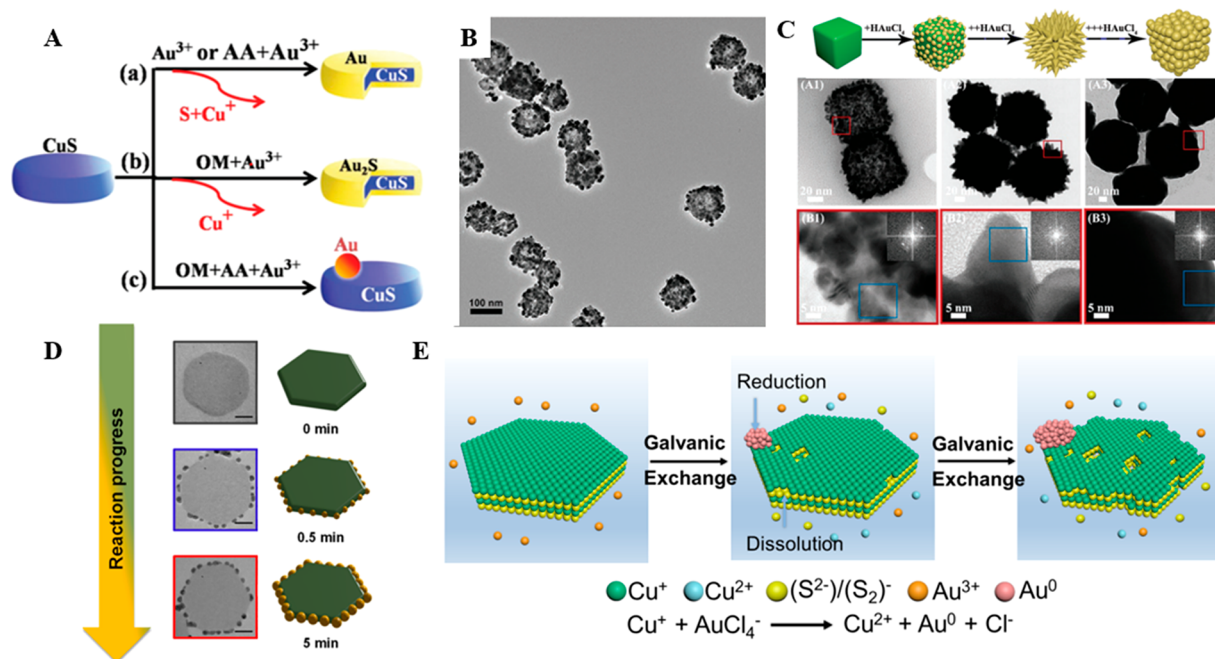


Figure 7. (A) Sketch of the various reaction conditions and related heterostructures involving the as-synthesized CuS NCs and Au^{3+} ions at room temperature. Reproduced and adapted with permission from ref 75. Copyright 2018 Royal Society of Chemistry. (B) TEM image of HCCuS@Cu₂S@Au nanoshell/satellite nanoparticles. Reproduced and adapted with permission from ref 76. Copyright 2017 John Wiley and Sons. (C) Schematic illustration of the synthesis of HCCuS@Au core-shell NPs with different morphologies of Au shell and TEM images of HCCuS@Au NPs (A1), HCCuS@spiky Au NPs (A2), and HCCuS@islanded Au NPs (A3), respectively. High-magnification TEM images (B1–B3) and the corresponding FFT patterns (insets) of HCCuS@dotted Au NPs, HCCuS@spiky Au NPs, and HCCuS@islanded Au NPs, respectively. Reproduced and adapted with permission from ref 77. Copyright 2018 Royal Society of Chemistry. (D) Left section shows HRTEM images in the top view of the CuS NPLs after different time intervals of the gold growth process (scale bars: 5 nm). The right section schematically illustrates the morphological evolution of the CuS@Au hybrid structure within the first 5 min of the reaction. Reproduced and adapted with permission from ref 78. Copyright 2022 American Chemical Society. (E) Galvanic exchange-induced growth mechanism of Au nanocrystal on CuS nanoplate. Reproduced and adapted with permission from ref 80. Copyright 2019 Elsevier.

components. Au core NPs of various shapes and sizes could be used to modify the LSPR properties of final nanostructures.⁷³ The hybrids designed based on nanorods demonstrated enhanced NIR extinction caused by overlapping plasmon responses from two components and by the plasmon-induced resonance energy transfer (RET) process.

Another parameter greatly influencing the optical properties of hollow dual plasmon nanostructures is the final shell thickness. Thicker shells were found to diminish Au core LSPR response.⁷² The size of the interior voids and outer copper chalcogenide layer could be modulated by the nature and concentration of the chalcogenide precursor in the reaction mixture.⁷⁴ Organic molecules thioacetamide and 1,1-dimethyl-2-selenourea were used as the source of chalcogenide anions to form hollow Au@Cu_{2-x}S and Au@Cu_{2-x}Se nanocomposites, respectively, under identical conditions. The addition of those precursors at elevated temperatures enabled the conversion of Au@Cu₂O into the hollow nanostructures because of the thermal decomposition of the chalcogenide source, which ensured a sufficient amount of chalcogenide in the reaction mixture. However, in the case of hollow Au@Cu_{2-x}S, the Cu₂O shell was only partially converted, and part of it remained attached to the Au core. This could be explained by the formation of a dense Cu_{2-x}S shell due to aging processes, which prevented inward diffusion of S²⁻ and ended the shell transformation. The structural differences of produced hollow Au@Cu_{2-x}Se and Au@Cu_{2-x}S nanostructures explained their distinct optical responses in visible spectral range and were

reflected in TEM and EDS elemental maps (Figure 6F,G). Signal distribution in the EDS mapping images of the Au@Cu_{2-x}S NPs reveals Cu presence at the edge and in the center, while the S signal mainly locates at the surface of heteronanostructures, which is another evidence of the Cu₂O presence. However, complete transformation into hollow Au@Cu_{2-x}S was reported using ionic compounds, such as Na₂S.^{70,73}

3.4. Reversed Satellite Structures. An alternative design of a noble metal-copper chalcogenide nanostructure is the heteronucleation of gold on the surface of the semiconductor shell. Reaction conditions are the determining factor of the heterostructure type achieved.⁷⁵ CuS@Au core-shell structures were formed in the reaction of CuS NCs with Au^{3+} ions, regardless of ascorbic acid presence (Figure 7A). The same reaction with the addition of oleylamine results in CuS@Au₂S core-shells because of active cation exchange between the gold and copper ions in those conditions. Au/CuS dimers were produced in the reaction with oleylamine and ascorbic acid. The ascorbic acid serves as a reducing agent to convert Au^{3+} to Au^0 , which is deposited on the CuS surface. HAuCl₄ as a gold precursor has been reduced to form the spherical gold nanoparticles, which were uniformly deposited on the hollow CuS NPs in the presence of thiol-polyethylene glycol amine to produce hollow CuS@Cu₂S@Au core-satellite hybrids (Figure 7B).⁷⁶ The other reported structure was constructed of hollow CuS nanocubes, obtained from solid Cu₂O nanocubes, and an Au shell deposited on copper sulfide by the reduction of HAuCl₄ by ascorbic acid. As the amount of

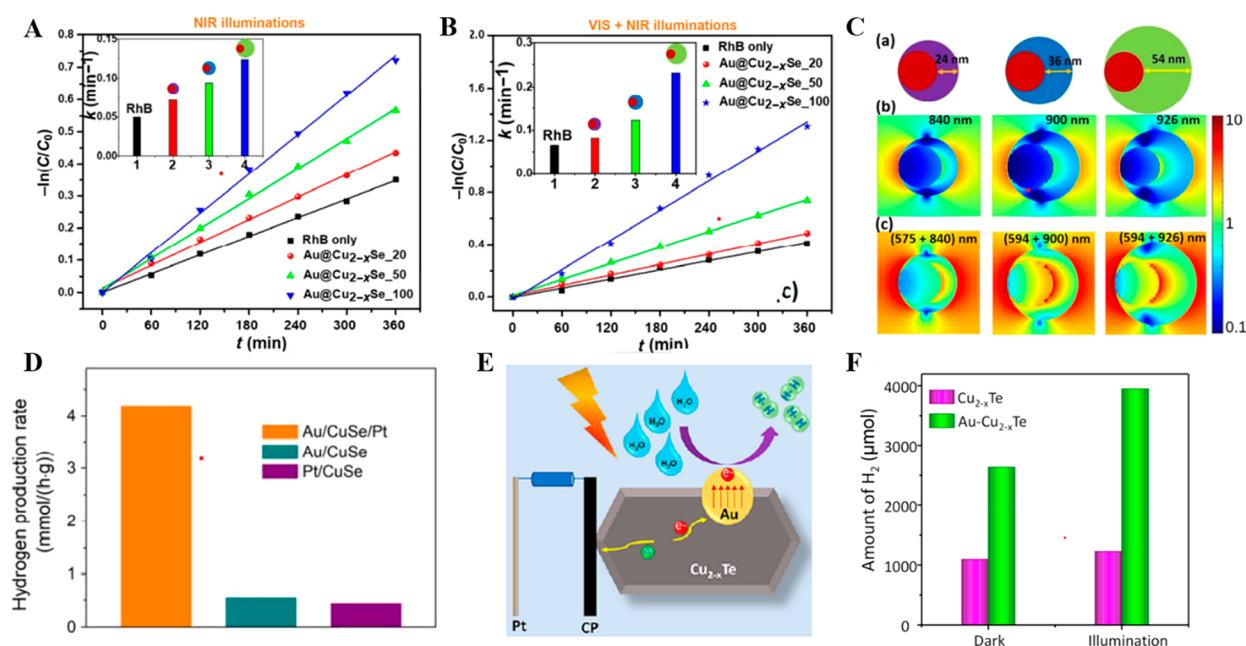


Figure 8. (A) First-order kinetics for RhB degradation under NIR illumination ($\lambda > 760$ nm) using Au@Cu_{2-x}Se nanoparticles of various shell thicknesses as catalysts. (B) First-order kinetics for RhB degradation under visible and NIR illumination ($\lambda > 420$ nm) using Au@Cu_{2-x}Se nanoparticles of various shell thicknesses as catalysts. Insets illustrate the values of rate constants of corresponding reactions in the absence and presence of Au@Cu_{2-x}Se with 3 different shell thicknesses. (C) The near electric field maps of the eccentric Au@Cu_{2-x}Se NPs. (a) Schematics of the computational models of the Au@Cu_{2-x}Se nanoparticles. (b) Spatial distribution of the local electric field enhancement ($|E/E_0|$) of the three nanoparticles excited at a single wavelength. (c) Spatial distribution of the local electric field enhancement ($|E/E_0|$) of the three nanoparticles excited at a dual wavelength. The excitation wavelengths are indicated on each panel. Reproduced and adapted with permission from ref 17. Copyright 2021 Springer Nature. (D) Comparison of the hydrogen production rate of Au/CuSe/Pt, Au/CuSe, and Pt/CuSe hybrids. Reproduced and adapted with permission from ref 81. Copyright 2019 John Wiley and Sons. (E) Schematic illustration of the HER mechanism on the surface of Au–Cu_{2-x}Te disk-on-dot heterostructures. (F) Bar diagrams of the amount of H₂ obtained under dark and illumination in 0.5 M H₂SO₄ using Cu_{2-x}Te and Au–Cu_{2-x}Te nanocrystals. Reproduced and adapted with permission from ref 55. Copyright 2021 American Chemical Society.

gold precursor increased, the morphology of the Au shell changed from dots to branches to islands (Figure 7C).⁷⁷ Different architecture of hollow cubic CuS@spiky Au core-shell NPs with “tip spots” on the surface generated an enhanced electromagnetic field and increased light absorption.

Recently, the delicate synthesis of side-selective gold growth on the CuS nanoplatelets in the presence of oxalic acid and oleylamine in darkness was demonstrated.⁷⁸ By varying the reaction time while the other parameters were kept the same, the number, size, and interparticle distance between the gold nanoparticles could be adjusted (Figure 7D). The key factor for preferential growth at the sides of copper sulfide was the exposed disulfide bridges of the covellite, which possess a high affinity to gold. Also, Au NPs were formed on the basal planes of CuS nanoplatelets under illumination, showing the parallel reduction path of the gold-source based on photoreduction. Such a green technique as photochemical reduction of HAuCl₄ was successfully employed to form Au NPs on the surface of CuS avoiding the addition of any reducing agent.⁷⁹ Besides direct AuCl₄⁻ ions reduction in solution and photocatalytically, gold nanoparticles could be deposited on the CuS cores by a galvanic exchange route (Figure 7E). CuS nanoplates have been used as effective nanoplatforms and reducers for the production of CuS–Au heterostructures through the galvanic exchange at ambient temperature without the additional reducing agent or organic solvent.⁸⁰ The *in situ* growth of Au NPs was initiated after the introduction of CuS nanoplates into HAuCl₄ aqueous solution under continuous stirring. Part of CuS nanoplates are partially oxidized and dissolved into the

solution, while AuCl₄⁻ ions are reduced to metal Au, which nucleate and grow on the surface of CuS. The quantity and the size of Au nanocrystals on the CuS nanoplate were controlled by adjusting the Au/Cu molar ratios and stirring time.

4. APPLICATIONS

Promising applications of dual plasmonic heteronanostructures are discussed in this section. The localized surface plasmon resonance is known to enhance the efficiency of various processes and devices in photocatalysis, photovoltaics, sensing, imaging, and biomedicine.

4.1. Photocatalysis. Noble metal–nonstoichiometric copper chalcogenide heteronanostructures demonstrate much better photocatalytic activity than a single component. The plasmonic coupling between two dissimilar optical resonances of eccentric dual plasmonic Au@Cu_{2-x}Se hybrid nanocomposites was studied experimentally and theoretically. Photocatalytic experiments were conducted under 3 conditions: in darkness, under sole excitation of Cu_{2-x}Se NIR LSPRs, and under dual (visible and NIR) simultaneous excitation of Au and Cu_{2-x}Se LSPRs (Figure 8A,B). The photocatalytic reaction rate was found to be higher under dual excitation than with sole NIR excitation, which was assigned to the effect of plasmonic coupling and high local electric field enhancement at the interface of heteronanostructures. The conclusion was confirmed by the output of FDTD calculations showing that excitation of both constituent LSPRs results in a stronger local electric field enhancement at the interface than that upon sole NIR excitation, when only the semiconductor

becomes active (Figure 8C). Also, the modeled electric field distribution around hybrid nanostructures under the visible light range when only Au LSPRs are photoexcited exhibited a lower local electric field enhancement compared to dual excitation. Photocatalytic efficacies of Au@CuS core-shell NPs and bare Au NPs were compared experimentally as well.⁴⁴ In the condition of the Au LSPR excitation with the incident light of a resonant frequency, Au@CuS core-shell NPs exhibited higher photocatalytic activity than Au NPs due to effective charge separation and longer hot carriers' lifetime.

The power dependence of reaction rates was further explored.⁴⁴ The rate constant of photocatalytic mineralization of RhB driven by d-to-sp interband excitation exhibited excitation power dependence strikingly distinct from that of the plasmon-driven photocatalytic activities. The linear relationship between the rate constant and excitation power was observed under weak excitations ($P_{\text{ex}} < 0.8$ W) for interband exciton-driven photocatalytic reactions, while a significant deviation from the linear dependence became predominated with the excitation power set above 2.0 W. The experimentally observed deviation, especially the asymptotical evolution approaching the plateau was interpreted as the consequence of saturated optical excitations of the interband transitions. On the contrary, photocatalytic reactions under the excitation of plasmon strictly followed the linear dependence essentially due to the substantially shorter lifetimes and faster decay of the plasmonic hot carriers in comparison with those excitonic electron-hole pairs. The effect of excitation power on the quantum efficiencies was investigated by the authors. Interestingly, the quantum efficiencies in the regime with a low excitation power were independent of P_{ex} but approximately 1 order of magnitude higher than those of plasmon-driven reactions because of the long-lived excitonic carriers rather than the plasmonic hot carriers. The similar saturation of optical excitation resulted in a remarkable drop in quantum efficiencies by more than 75% when the excitation power increased above 2.0 W in their experiments. The photocatalytic efficacies of Au@CuS dual plasmonic nanoparticles were compared to those of bare Au nanocrystals and the lower photocatalytic activities from Au under excitation of LSPRs in the visible region indicated the beneficial charge separation and increased lifetimes of the charge carriers caused by the transfer of plasmonic hot carriers across the metal-semiconductor interface during the photocatalytic molecular transformation. Although how the plasmonic hot carriers in dual plasmonic heteronanostructures behave differently from the excitons still remains elusive, noble metals serving as the electron sink might promote the charge separations in the excitons. These insights can serve as guiding principles for the rational design of multiplasmonic heteronanoarchitectures with optimized and synergistic optical properties for photocatalytic applications.

Pt decorated Au/CuSe hybrids were carefully designed to produce strong dual plasmon resonance for photocatalytic hydrogen generation from water splitting with visible light ($\lambda > 420$ nm) irradiation.⁸¹ To form the dual plasmonic structure for light harvesting and near-field enhancement, CuSe ultrathin nanoplate was grown on the Au nanospheres by a hydrothermal method. Pt nanoparticles are deposited on presynthesized nanocomposites to serve as cocatalysts for hydrogen reactions. Photocatalytic hydrogen generation activity of Au/CuSe/Pt hybrid nanocomposites was 7.8 and 9.7 times higher than that of Au/CuSe and Pt/CuSe, respectively (Figure 8D).

An Au-Cu_{2-x}Te disk-on-dot heteronanostructure has been successfully employed as a photoelectrocatalyst for hydrogen evolution reactions (HERs) (Figure 8E).⁵⁵ Its superior activity compared to pristine Cu_{2-x}Te was demonstrated by linear sweep voltammetry. Au-Cu_{2-x}Te required a lower overpotential of 282 mV to reach the current density of 10 mA/cm², while for pure Cu_{2-x}Te 454 mV was needed. To evaluate the efficiency of the electrocatalysts, electrochemical hydrogen evolution reactions were performed in the presence of Au-Cu_{2-x}Te and pure Cu_{2-x}Te NPs in dark and illuminated conditions. The amount of produced hydrogen gas under dark and illuminated conditions in the presence of Au-Cu_{2-x}Te and pure Cu_{2-x}Te was compared (Figure 8F). The maximum amount of gas of about 3948 mmol was produced for Au-Cu_{2-x}Te under illumination, which was higher than that under dark conditions. The higher activity of Au@Cu_{2-x}Te disk-on-dot heteronanostructures was explained by the presence of a more electron-abundant Au core enriching the concentration of hot electrons and providing additional sites for hydrogen ion reduction. Merging Au and Cu_{2-x}Te into a single heteronanostructure allowed the production of a hot electron and holes with a prolonged lifetime enhancing their photocatalytic performance in HER.

4.2. Biomedicine. Nonstoichiometric copper chalcogenides provide plasmon absorption into the second NIR biowindow at sizes below 100 nm, making dual plasmonic heteronanostructures suitable materials for utilization in biomedicine, including photothermal and photoacoustic imaging, cancer radiotherapy, drug delivery, etc.¹⁸ Chemodynamic therapy (CDT) is one of the actively investigated approaches for cancer treatment and based on the Fenton type reactions between transition metal ions (e.g., Fe²⁺, Mn²⁺, Cu⁺) and intracellular H₂O₂ to produce •OH because the high reactivity and short life of hydroxyl radicals provide tumor-area specificity and low invasiveness. Therefore, chemical reactions that actively produce hydroxyl radicals from H₂O₂ within a cell are highly desired. Also, Cu⁺-catalyzed Fenton-like reactions have been shown to be superior to Fe²⁺/Fe³⁺ in both kinetics and energy in neutral and weakly acidic tumor environments.⁸² Recently, a dual plasmonic Au@Cu_{2-x}S nanoreactor has been formed by covalent immobilization of defective Cu_{2-x}S quantum dots onto the surface of Au nanoparticles capped in silk fibroin and demonstrated enhanced reactive oxygen species generation.⁸³ Among copper chalcogenides, improved antioxidant activity, high biocompatibility, and low toxicity have been detected in copper selenide.^{84,85} Au@Cu_{2-x}Se heterogeneous nanostructures have been demonstrated to assist Fenton-like reactions generating •OH from H₂O₂ and photothermal conversion due to strong NIR extinction. Extra •OH can be effectively formed by the photocatalytic reaction induced by excited plasmonic holes from dual plasmonic Au@Cu_{2-x}Se nanosystems.^{54,86} Interestingly, when comparing the generation of OH radicals mediated by amorphous Au@Cu_{2-x}Se hybrid particles with those containing Cu_{2-x}Se in a highly crystalline form, the first type showed higher photocatalytic efficiency.⁵⁶

To improve the antitumor efficacy, chemotherapy is used together with photothermal therapy (PTT), which converts external near-infrared light into heat to ablate tumors. The rational design of photothermal agents at the nanoscale has a high priority among material researchers to improve cancer treatment and bacteria cells damage by efficiently converting incident energy into heat. Efficient photothermal ablation of

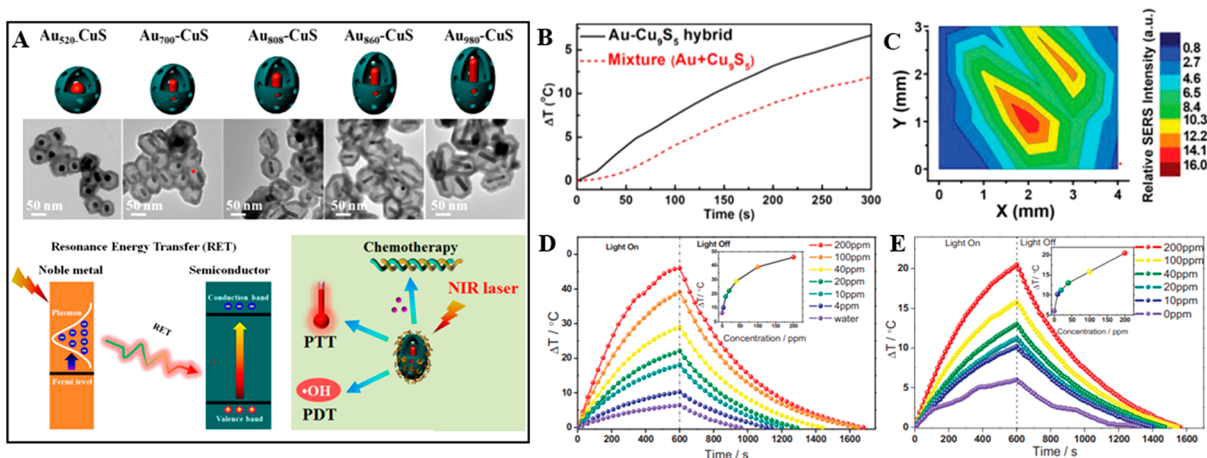


Figure 9. (A) Illustration of Au–CuS yolk–shell NPs and their TEM images. Resonance energy transfer process that does not require the metal–semiconductor interface. Applications of multifunctional Au–CuS yolk–shell NPs for chemophototherapy of cancer. Reproduced and adapted with permission from ref 73. Copyright 2018 American Chemical Society. (B) Temperature elevation profile of Au–Cu₉S₅ and the physical mixture of Au and Cu₉S₅ NPs at the same concentrations. Reproduced and adapted with permission from ref 15. Copyright 2014 American Chemical Society. (C) The contour of relative SERS intensity of the tumor region. Reproduced and adapted with permission from ref 89. Copyright 2018 John Wiley and Sons. (D) PT conversion characterizations of Au@Cu_{2-x}S NRs water colloid with various concentrations by 1 W cm⁻² 808 nm laser and by (E) 0.7 W cm⁻² 1064 nm laser irradiation for 10 min, the insets show the temperature increase (ΔT) at different concentrations. Reproduced and adapted with permission from ref 61. Copyright 2016 John Wiley and Sons.

cancer cells is challenging because of the relatively low photothermal conversion efficiency. To achieve the effective heating effect, the strong plasmonic extinction of nanomaterials serving as photoabsorbers in the NIR region is imperative. Au–Cu₉S₅ hybrid NPs demonstrated about 50% absorption enhancement at 1064 nm compared to the physical mixture of Au and Cu₉S₅ NPs due to the plasmon hybridization in Au–Cu₉S₅ hybrid system, which includes both free electron-based LSPR in the Au domain and free hole-based LSPR in the Cu₉S₅ domain.¹⁵ Also, the improved photothermal heating effect of Au–Cu₉S₅ hybrids compared to the simple sum of individual components with the same concentration of Au and Cu was shown (Figure 9B). Obtained photothermal transduction efficiency of Au–Cu₉S₅ hybrids was around 37%, which makes them excellent nanoheaters for *in vitro* and *in vivo* cancer cells photothermal ablation in the NIR-II window. When exploring heat generation by Au@Cu_{2-x}S nanostructures dispersion, the temperature of hybrids increased faster than that of Au NPs, Cu_{2-x}S NPs, or their physical mixture as well.⁵⁴ Improved photothermal performance of Au@Cu_{2-x}S nanocomposites was ascribed to a strong LSPR coupling between Au and Cu_{2-x}S and enhanced the NIR absorption.⁸⁷

Spectral response of dual plasmonic nanocomposites can be manipulated by the size of the core, the aspect ratio of anisotropic Au NPs, the doping level of the copper chalcogenide shell, and its thickness. Dual plasmonic heteronanostructures permit independent morphology control of the Au core and shell, therefore the Au core could be easily tailored from spherical into a nanorod shape. Also, the deposition of a semiconductor shell on a prefabricated core provides the advantage of flexible shell thickness tuning. A series of Au cores with different LSPR frequencies were embedded in hollow CuS shells to achieve an efficient photothermal effect through the RET process (Figure 9A).⁷³ The highest photothermal performance can be achieved in hollow Au–CuS nanosystems by tuning the LSPR peak of Au cores to match the wavelength of the laser. Hollow dual plasmonic heteronanostructures concentrate the incident light

into “hotspots” and produce local electromagnetic field enhancement initiating RET from plasmonic metal to semiconductor (Figure 9A). When the wavelength of incident light matches the LSPR peak wavelength of plasmonic metal core, the energy is transferred from Au core to CuS shell greatly increasing the electron–hole pair magnitude in the CuS shell. Therefore, the RET process generated excited electrons in the CuS shell enhancing the photothermal performance of hollow Au@CuS nanocomposites, while the increased hole density in the valence band produced more •OH radicals improving photodynamic properties and small molecules could be loaded into the void space for the potential chemotherapy (Figure 9A). In the other work, LSPR properties of the aqueous dispersions of Au@Cu_{2-x}S NRs have been tailored and such nanomaterials demonstrated the PT conversion efficiency of 59% under irradiation by 1 W cm⁻² 808 nm light and 43.25% under irradiation of 0.7 W cm⁻² 1064 nm light (Figure 9D,E).⁶¹

Au@Cu_{2-x}S NRs have been reported to effectively degrade A β 1–42 fibrils into amorphous protein.⁸⁸ A β could be one of the causes of Parkinson’s and Alzheimer’s disease; therefore, effective A β 1–42 degradation is critical. Au@Cu_{2-x}S core–shell NRs have demonstrated the potential to decrease the aggregation and toxicity of A β 1–42 due to higher photothermal transduction efficiency induced by strong coupling between the two kinds of LSPR effect in the NIR region. While photothermal conversion efficiencies for the Au NRs and Cu_{2-x}S colloidal solutions were 32.3% and 29.3%, respectively, it reached 60.2% for Au@Cu_{2-x}S core–shell NRs, which further proves the superiority of the material for light-to-heat induced molecule degrading process.

In addition to the photothermal effect, such multifunctional dual plasmonic nanomaterials own imaging functionalities based on the surface-enhanced Raman scattering (SERS) due to the tailored localized surface plasmon resonance coupling between the noble metal core and semiconductor shell.⁸⁹ Au@Cu_{2-x}S NPs with folic acid adsorbed on their surface for the accurate discrimination of normal epithelial cells from cancer

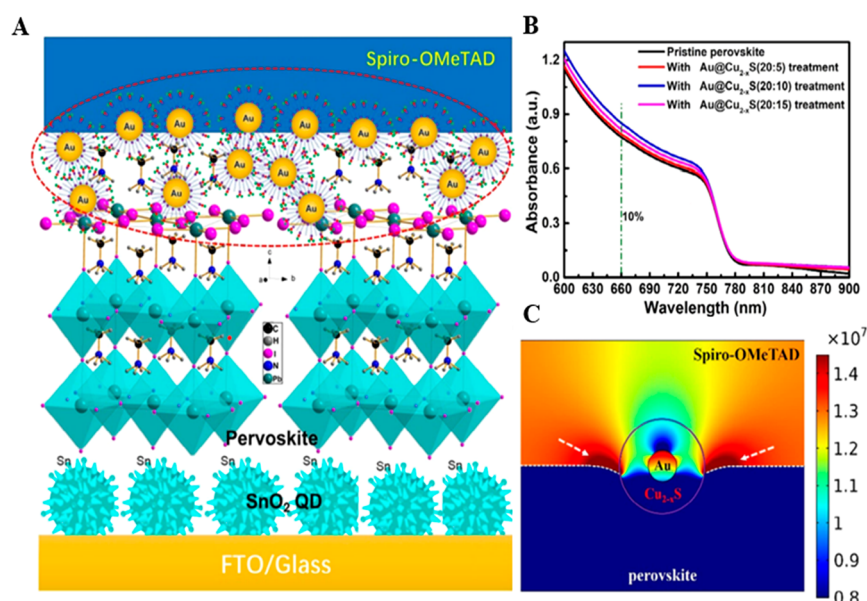


Figure 10. (A) Illustration of the Au@Cu_{2-x}S NPs present at the spiro-OMeTAD/perovskite interface. (B) Absorption spectra of perovskite with Au@Cu_{2-x}S treatment. (C) Simulation of the electrostatic field of Au@Cu_{2-x}S interface between spiro-OMeTAD and perovskite under a potential of 1.1 V. Reproduced and adapted with permission from ref 90. Copyright 2021 John Wiley and Sons.

cells were utilized for efficient tumor ablation therapy guided by SERS imaging. After Au@CuS-FA NPs injection, the tumor region of the mouse was examined by SERS mapping (Figure 9C). The relative SERS intensity decreased from the tumor center to the surrounding normal tissues, which allow precise localization of the tumor area. Moreover, the PT conversion efficiency of the Au@CuS core-shell NPs further improved and reached 45%. Hence, Au@CuS core-shell NPs could be effectively used for diagnostics, therapeutics, as well as treatment response monitoring by utilizing SERS as a navigation tool.

4.3. Perovskite Solar Cells. Dual plasmonic nanomaterials exhibit tremendous potential in energy-related applications. Au@Cu_{2-x}S heteronanostructures enhance the infrared absorption and intensify the local electric field at the perovskite/spiro-OMeTAD (2,2',7,7'-tetrakis[*N,N*-di(4-methoxyphenyl)amino]-9,9'-spirobifluorene) interface of collar cells (Figure 10A,B).⁹⁰ Also, the absorbance in the UV-visible region slightly increased compared with the pristine perovskite film. These mesoporous NPs contact sufficiently with spiro-OMeTAD, the hole transport layer material, to form channels for hole extraction and act as “bridges” for hole transfer. Thus, interfacial treatment with Au@Cu_{2-x}S nanocomposites enhanced the hole mobility and device stability. The electrostatic field simulation at the perovskite/spiro-OMeTAD interface revealed the intensification of the electric field at the perovskite–Au@Cu_{2-x}S nanostructures–spiro-OMeTAD interface, which could be explained by a high concentration of hole carriers transferred from Au@Cu_{2-x}S to spiro-OMeTAD (Figure 10C). The electric field weakening occurs in the region above the core-shell Au@Cu_{2-x}S NPs. Au@Cu_{2-x}S nanostructures can be filled into the grain boundaries of perovskite to passivate the interface defects as well as improve the contact properties at the perovskite/spiro-OMeTAD interface to accelerate the hole extraction. Such Au@Cu_{2-x}S-based perovskite collar cell displayed an efficiency of 22.15% with negligible hysteresis.

The utilization of dual plasmonic hybrid nanostructures in perovskite solar cells (PSCs) can shed light on the correlation between the structural parameters and the trap-filled limit voltages used to determine the trap density. The mechanism of the passivation of the surface defects at the interface between the perovskite film and the organic semiconductor in a PSC through the modulation of valence-band offset by the dual plasmonic nanoarchitectures can also be elucidated in detailed work to facilitate and promote the hole extraction. Moreover, through the systematic studies on the charge transport parameters, including charge transfer resistance and recombination resistance obtained from the electrochemical impedance spectroscopy (EIS), the power conversion efficiencies and operational stabilities of perovskite solar cells can be optimized by the capabilities of dual plasmonic nanostructures in suppressing the charge recombination and moisture invasion, respectively. Benefiting from the enhanced NIR light absorption, the high-efficiency solid-state perovskite solar cell integrated with versatile dual plasmonic nanoparticles will possess superior performance over commercial silicon or other organic solar cells and become a strong candidate for a next-generation solar energy harvester.

4.4. Upconversion Nanoparticles. Au–CuS heterodimer nanocrystals were utilized to enhance the upconversion luminescence intensity of Yb/Er-codoped NaGdF₄ NPs.⁴⁶ An enhanced electric field, created by dual plasmonic NPs, intensifies the emission of the nearby upconversion nanoparticles (UCNPs) increasing the excitation rate when the LSPR frequency matches the absorption of sensitizer or stimulating the radiative decay rate, the so-called Purcell effect when the plasmon resonances match the emission of the activator. While the Au core was synthesized with a size below 20 nm to support the LSPR peak at 520 nm, matching the emissions of Er³⁺, the LSPR peak of CuS could be tuned to 980 nm to correspond to the absorption of Yb³⁺. Au–CuS heterodimers enhanced the luminescence of NaGdF₄:Yb/Er UCNPs by 17.5-, 6.4-, and 7.4-fold at 520, 540, and 654 nm,

respectively, which outperformed the single plasmonic component of Au or CuS.

The plasmon-enhanced upconversion photoluminescence is a multistep process composed of long-lived intermediate states, and the intensity of photoluminescence is modulated by the competition between the radiative decays and nonradiative energy transfer from the excited state to the ground states. The hybridization of dual plasmonic nanostructures with UCNPs provides an ideal platform for the investigation of the energy transfer process between the emitter and the locally enhanced electromagnetic fields induced by two mechanistically distinct LSPRs, which helps us develop an in-depth understanding of the contributed effect of the modified relaxation rate of the emitter toward the radiative emission rate. Moreover, fundamentally important questions, such as the configuration and the distance between the dual plasmonic nanocrystals and UCNPs, the spectral overlap between the extinction of dual plasmonic particles and emission/excitation of UCNPs, the effect of the chemical composition of dual plasmonic nanoarchitectures on the energy transfer efficiency, and the electromagnetic-field dependence of the upconverted luminescence process, can be clearly and quantitatively answered with the coupling of these two optically active components at the nanoscale. Studies based on the integration of dual plasmonic nanostructures with UCNPs pave the way for the further development of hybrid nanomaterials with architectural complexities and hold great promise for widespread applications in spectroscopy, bioimaging, photothermal therapy, and smart devices in sensing.

5. SUMMARY AND PROSPECTS

In conclusion, considering various nanomaterials that exhibit LSPR properties, such as noble metals and doped semiconductors, it is beneficial to combine them into one unit to maximize the synergistic plasmonic coupling effects. This review is focused on recent research findings on noble metal–nonstoichiometric copper chalcogenide nanostructures. Although researchers have been synthesizing hybrid nanocomposites for decades, precise control over the morphology and architecture of produced heterostructured and mono-dispersed nanoparticles remains highly challenging. The composition, size, and geometry of both constituents are dominant factors determining plasmonic and physicochemical properties. Therefore, various synthetic strategies to obtain dual plasmonic nanostructures of different architectures were discussed. A carefully elaborated fabrication approach permits the tuning and optimization of optical and structural properties for widespread applications.

The plasmon coupling between the electrons and holes in a hybrid dual plasmonic heteronanostructure is still ambiguous and not fully understood since research on the crosstalk at the nanoscale between two dissimilar building blocks of noble metals and nonstoichiometric copper chalcogenides is still at a rudimentary stage. One of the interesting works published earlier this year studied the unique dynamics and the temporal evaluation of plasmon coupling-induced charge carriers with time-resolved ultrafast transient absorption spectroscopy (TAS) in dual plasmonic Au/CuS nanocrystals.¹⁶ Although the authors claimed the probed bidirectional interaction under resonant excitations in two constituent domains of Au and CuS occurred as an energy transfer or charge carrier transfer based on the transient observations of the almost identical decay dynamics of the hot charge carriers in the same hybrid

nanostructure, the way the two mechanistically distinct plasmon resonances couple to each other and the migration/direction of two different charge carriers (electrons in Au and holes in CuS) at the interface on the time scale of femtosecond was still not clearly elucidated due to the temporal resolution restraints for both dephasing and thermalization processes. Another previously published work examined the similar transient bleaching dynamics of the intrinsic gold and copper selenide LSPR bands in asymmetric Au@Cu_{2-x}Se crescent-like nanostructures with TAS techniques.⁹ Such exponentially decreased bleaching amplitudes of the intrinsic transient absorption signals in respective Au and Cu_{2-x}Se domains caused by the fast carrier-phonon scattering and slower phonon–phonon relaxation during the heat dissipation indicated the plasmon coupling between the constituent domains. Based on the fitted bleaching dynamics of hybrid Au@Cu_{2-x}Se with varying Cu_{2-x}Se: Au molar ratios, they claimed the transfer of electrons from Au domains to the Cu_{2-x}Se domain with the increasing molar ratios during the plasmon coupling processes. However, under the condition of off-resonant excitations, the conclusions they made on the transfer direction of electrons in dual plasmonic Au@Cu_{2-x}Se was impertinence and not fully evidenced or reasonably supported by the experimentally determined results on the bleaching amplitudes. For example, the decreased bleaching amplitude of the intrinsic TA signal in the Au domain with the increase of Cu_{2-x}Se: Au molar ratios could be caused by the weaker electromagnetic fields instead of decreasing electron density proposed by the authors. Redshifts of Au LSPRs were observed in the extinction spectra due to the increased refractive index of the thickened Cu_{2-x}Se shell, which in turn lengthened the spectral distance between Au LSPRs and the excitation source of a 380 nm pump pulsed laser. This results in a weakened electromagnetic field and the generation of excited electrons with reduced concentrations and densities. On the same token, the bleaching amplitude of the intrinsic TA signal of Cu_{2-x}Se domains that linearly increased with Cu_{2-x}Se: Au molar ratios was not completely ascribed to the migration or transfer of electrons. The enlarged NIR extinction cross section as a result of the gradually increased shell thickness slowing down the phonon–phonon relaxation processes might contribute to the observed bleaching behaviors. Therefore, the plasmon coupling and the associated charge-carrier migration in dual plasmonic hybrid heteronanostructures under resonant excitations are still underexplored with debating and even controversial open questions that are well-worthy of in-depth investigations. Moreover, the efficient plasmon coupling in photocatalysis needs to be systematically studied with the integration of ultrafast transient, steady-state absorption, and compelling numerical simulations to help us develop a quantitative understanding of the underlying mechanisms and photophysical processes. Most majorities of the current studies are based on eccentric core–shell nanoparticles, more case studies using dual plasmonic hybrid nanostructures with well-controlled morphologies and architectural complexities, such as hollow structures, need to be carried out to help us complete the puzzle in plasmon coupling by providing insights into the mechanisms of photocatalysis and photophysical processes. The coupling strength in dual plasmonic nanoparticles can be experimentally tuned through deliberate architectural design and synthesis to modulate the spectral overlapping in the extinction spectra between noble metal LSPR bands and those of copper

chalcogenides in the same nanostructure. Noble metal nanostructures with anisotropic morphologies, such as elongated nano bipyramids and hollow dual plasmonic nanoparticles, could be utilized to shift the LSPRs toward NIR spectral regions to enhance the crosstalk with the plasmonic chalcogenides. The study on the effect of the strengths of the plasmonic resonances on the coupling efficiencies is an alternative for tuning, such as the overgrowth of copper chalcogenides to silver nanoparticles with the most intensified LSPRs among the counterparts of noble metals. In the meanwhile, the synthetic approaches, such as template-mediated multistep fabrication and nanoscale Kirkendall Effect-promoted wet-chemistry methods need to be tailored and optimized for the construction of dual plasmonic nanoparticles with enhanced coupling strengths. The enhancement of the electromagnetic fields in dual plasmonic nanostructures can be assisted by the utilization of abundant low-frequency NIR light photons via hybridizing/integrating to other optically active nanomaterials with nonlinear characteristics, such as rare-earth-doped upconversion nanocrystals to ensure the optimal coupling.

Although considerable progress was made, the field of dual plasmonic noble metal–nonstoichiometric copper chalcogenide nanostructures is still at a pioneering level with numerous open questions, and further investigations are needed to address them.

5.1. Dual Plasmonic Heteronanostructures Based on Ag (Ag@Cu_{2-x}E). Plenty of studies have been published on dual plasmonic materials based on an Au core. However, other plasmonic metals need to be studied for the formation of such nanostructures. Silver is the most suitable candidate to enhance the plasmonic coupling effect between the core and shell because it shows a higher electromagnetic field enhancement than gold.⁵⁷ To further increase the coupling strength, anisotropic Ag NPs should be synthesized to red-shift the LSPR peak spectral position to that of the copper chalcogenide shell. The underlying challenge is to protect the Ag surface from oxidation during the shell deposition while preserving its outstanding plasmonic properties. It was shown that to suppress Ag oxidation, an ultrathin Au shell may be deposited on the surface of Ag nanocubes in the presence of a reducing agent and adjusted pH to prevent the galvanic replacement reaction.⁹¹ The thickness of the Au shell can be controlled on an atomic level and, most importantly, a few Au layers on the surface of Ag nanocubes do not change their plasmonic properties. It is expected that this approach will enable the fabrication of Ag@Cu_{2-x}E nanostructures.

5.2. Dual Plasmonic Heteronanostructures with Copper Telluride Shell (Au@Cu_{2-x}Te). The other direction is to extend the variety of shell materials and to develop synthetic approaches for coating plasmonic noble metals with copper telluride. Au@Cu_{2-x}S and Au@Cu_{2-x}Se are the most explored dual plasmonic heterostructures and studies of Au@Cu_{2-x}Te are very limited due to the lower abundance of tellurium and synthetic difficulties caused by a larger-sized anion. The topicality of the research related to Cu_{2-x}Te containing heteronanostructures is confirmed by an increasing number of recent publications.^{92,93} Cu_{2-x}Te were produced via partial anion exchange from Cu_{2-x}S NPs preserving their size or shape without inducing voids in the product nanoparticles. During this transformation, LSPR was initially quenched due to the formation of nonplasmonic stoichiometric copper chalcogenide nanoparticles and later plasmonic behavior

returned as the amount of Cu drops to form copper-deficient compounds.

The issues researchers may face are due to the wide lattice mismatch between the core material and Cu_{2-x}Te in the heterojunction. However, due to the optoelectronic properties and charge-transfer efficiencies, metal–telluride nanocrystals became promising nanomaterials for photoelectrocatalytic applications.⁵⁵ Heterostructures containing tellurides exhibit intriguing properties because tellurium is less electronegative in comparison to other chalcogenides. The metalloid behavior of tellurium promotes anisotropic structural growth. This feature of tellurides would permit the formation of dual plasmonic nanocomposites with tuned sizes, geometries, and morphologies of the shell, which is important not only from an architectural standpoint but also for tailoring their LSPR frequencies. Metal–tellurides have a lower energy bandgap; hence, the absorption band is positioned closer to longer wavelengths making them suitable for solar-energy-harvesting related applications.⁹⁴

5.3. Architectural Design through Site-Selective Overgrowth. The architectural design of nanomaterials is important for their prospective applications. For example, in core@shell nanostructures, the metal core is completely buried into the semiconductor and generated charge carriers have to diffuse through the shell to the surface to engage in the reaction, which makes them hardly accessible. On the other hand, a spatially separated geometry allows hot holes and electrons to be instantly and easily accessed by reactant molecules, usually resulting in improved photocatalytic activity. Therefore, selective-area growth is very important for the modulation and enhancement of certain functionalities. Production of a dual plasmonic nanostructure with anisotropic cores and a site-selective semiconductor shell deposition has not been thoroughly investigated and may be crucial for the appearance of new properties. Selective-area growth includes two steps: initial deposition of a shell material on specific regions of the core surface, which usually have been appropriately modified previously, and its subsequent growth. Selective overgrowth of plasmonic Cu_{2-x}E nanocrystals on gold remains a great challenge because of the difficult control of both nucleation and growth dynamics. One of the approaches to overcome this issue could be a selective deposition of Cu₂O following its transformation to chalcogenide through the nanoscale Kirkendall effect. Tunability of anisotropic overgrowth Cu₂O on Au NPs, the so-called Janus configuration, has been already performed using a strong thiol ligand to control interfacial energy.⁹⁵ Addition of 5-amino-2-mercaptobenzimidazole (AMBI) in various amounts influences the functional design of Au–Cu₂O hybrids, which could be further converted into dual plasmonic nanostructures. In addition, the other important morphological parameters like shell crystallinity and porosity can be tailored in a highly precise and controllable manner.⁹⁶ The final single crystal dense shell or polycrystalline porous hierarchical structure of Cu₂O could be precisely controlled via thermodynamic maneuvering, providing the opportunity to produce corresponding chalcogenide shells by anion exchange and to study the porosity effect, available surface sites and coordination environments on the resulting properties of the hybrid dual plasmonic nanohybrids. The ability to precisely control the structure–function relationships of these heteronanostructures gives rise to numerous and diverse applications.

5.4. Dual Plasmonic Nanostructures as Photocatalysts for Nitrogen Fixation. Recently, photocatalytic nitrogen fixation (PNF) has been investigated as an alternative to the Haber–Bosch path, which is a green approach to synthesizing NH_3 . The majority of current plasmonic nanostructures employed in photocatalysis are based on noble metals, which trigger hot-electron-driven reactions.^{97,98} For example, gold and silver NPs on doped $\text{g-C}_3\text{N}_4$ or Au NPs inside the UiO-66 MOF membrane have been successfully used in PNF. The hot electrons of the Au NPs surface were directly injected into the antibonding orbitals of N_2 molecules, which were also polarized by the induced electromagnetic field.⁹⁹ Besides that electrons can initiate the transformation of molecules adsorbed on the surface, they can be transferred to the semiconductor first through a plasmon-mediated electron-transfer (PMET) process. Also, oxygen vacancies in semiconductors have demonstrated a boosted N_2 activation effect. They induce a defect energy level, where metastable electrons can be localized and then moved to the antibonding orbitals of N_2 . Considering those facts and findings, dual plasmonic nanostructures, especially those converted from $\text{Au@Cu}_2\text{O}$ templates, present a high interest as nanophotocatalysts for PNF due to their plasmonic nature and the existence of ample oxygen vacancies. Moreover, the concentration of such active sites could be tuned during the transformation of copper(I) oxide to chalcogenide acquiring plasmonic properties simultaneously. Also, such dual plasmonic nanosystems would provide an opportunity to study the photophysical and photochemical processes involving hot holes driving oxidation reactions. Very few works have been dedicated to studying plasmonic hot hole transfer in plasmonic heterostructures.^{100,101} Moreover, the hole transfer mechanism remains unclear and requires detailed investigation.

5.5. Dual Plasmonic Nanostructures with Multi-component Copper Chalcogenides. Dual plasmonic heteronanostructures could serve as parent nanocrystals to create a myriad of novel nanomaterials preserving the size and shape, particularly through the transformation of the copper chalcogenide component. Ternary $\text{Cu}_{2-x}\text{S}_y\text{Se}_{1-y}$ nanosystems have shown tunable plasmonic properties between 1000 and 1600 nm.^{102,103} Recently, $\text{Cu}_{2-x}\text{Se}_{1-y}\text{Te}_y$ solid solutions were obtained as a result of partial tellurium anion exchange in weissite Cu_{2-x}Se nanoparticles with tunable tellurium content based on the amount of its precursor.¹⁰⁴ Therefore, combining such ternary semiconductors with noble metal NPs would form a new and unexplored type of dual plasmonic nanostructures. In addition, because Cu^+ ions in copper chalcogenides could be easily exchanged by other cations due to the small size and charge, cation-exchange reactions have become an alternative way to produce I–III–VI and I–IV–VI semiconductor domains of dual plasmonic nanostructures.¹⁰⁵ For example, Pd is slowly incorporated into the covellite nanocrystals, transforming their outer regions into an amorphous CuPd_xS shell that grows in thickness with an increase in the reaction time or amount of Pd precursor.¹⁰⁶ The LSPR position of nanostructures like $\text{Cu}_x\text{In}_y\text{S}_2$ and $\text{Cu}_x\text{Sn}_y\text{S}$ has been shown to depend on cation ratios,¹⁰⁷ which would allow property engineering within dual plasmonic nanomaterials after the elaboration of cation-exchange synthesis. The transformation from dual plasmonic to multicomponent plasmonic structures is one of the future burgeoning research directions. Vacancy-doped copper chalcogenide-based heteronanostructures with controllable sizes, shapes, morphologies, compositions, and

optimized physicochemical properties will become advantageous for a number of existing and novel nanotechnologies.

5.6. Surface-Enhanced Raman Spectroscopic (SERS) Sensing. Surface-enhanced Raman scattering is among the prospective applications of plasmonic nanomaterials. Dual plasmonic nanocomposites are ideal candidates for a molecular identification platform with SERS because the LSPR can be easily tuned by manipulating metal and semiconductor counterparts. Moreover, constructing such novel dual plasmonic nanostructures is promising for light-driven chemistry technologies and biosensing due to plasmon hybridization in the NIR region, which is valuable for biological applications providing deep penetration and minimal damage to the live tissues. Traditionally, gold and silver NPs were used in SERS, but their LSPR peaks are often limited to the visible spectrum.¹⁰⁸ Plasmon resonance frequencies of noble metals of large anisotropic NPs could be tuned into the desired range and demonstrate higher enhancement factors than spherical NPs.¹⁰⁹ However, only miniaturized devices utilizing NPs smaller than 100 nm will facilitate the adoption of SERS for medical applications. In recent years, degenerately doped semiconductors such as Cu_{2-x}E were successfully employed for SERS as well as showing efficiencies comparable to noble metals. For instance, plasmon-driven dimerization of 4-nitrobenzenethiol to 4,4'-dimercaptoazobenzene on Cu_{2-x}Se surfaces was monitored using the enhanced amplitudes of the Raman modes.¹¹⁰ Therefore, merging these two materials into one is very promising for SERS sensing, decreasing its detection limit, and increasing the sensitivity. Furthermore, the other types of dual plasmonic nanohybrids have been studied for their photocatalytic¹¹¹ and SERS¹¹² performance and demonstrated excellent capabilities due to the plasmonic coupling effect between plasmonic metal and heavily doped semiconductor.

5.7. Hybrid UCNP-Dual Plasmonic Nanosystems. Plasmonic nanomaterials have been actively employed as a part of complex nanostructures together with lanthanide-doped UCNP featuring NIR to visible anti-Stokes processes to enhance their upconversion luminescence. In such core–shell nanocomposites, plasmonic components create an enhanced electromagnetic field that leads to more efficient absorption, emission, and energy transfer processes.¹¹³ Plasmonic nanomaterials placed in close proximity to UCNP couple their plasmon resonance with either the excitation or the emission wavelength of the UCNP changing their anti-Stokes emission. To accomplish a signal enhancement LSPR of the plasmon, NPs have to match the excitation wavelength of the UCNP, increasing the excitation rate. Also, when the LSPR wavelength matches the emission wavelength of the UCNP, the Purcell effect takes place, increasing the radiative decay rate and luminescence. The luminescence enhancement is determined by the internanoparticle distance and nanoparticle size. The influence of the AuNP size in the 3.9–66 nm range on the upconversion luminescence has been investigated, revealing that for larger AuNPs the plasmon-induced luminescence enhancement process is dominant.¹¹⁴ Also, the effect of Cu_{2-x}S on the surface of UCNP was studied and the enhancement factors were found to be different from those with the metal nanostructure.¹¹⁵ The luminescence dependence on the Cu_{2-x}S particle size obeyed the same trend and the enhancement factor increased with the size of the Cu_{2-x}S NPs because the LSPR band was shifted toward the excitation wavelength. Hence, the development of new hybrid nanomaterials that

combine UCNPs and dual plasmonic NPs could further boost luminescence efficiency. In addition to the improvement of the luminescence, when the LSPR spectral position corresponds to the UCNP emission wavelength, a short-range nonradiative RET from the UCNP emitter ion to the plasmonic nanostructure occurs for subsequent initiation of photocatalytic or photothermal transformations. UCNPs have minimal background autofluorescence interference, high penetration depth, and spatial resolution; however, they possess a small absorption cross section and a low radiative decay rate. Therefore, upconverting nanoparticles covered with dual plasmonic nanostructures are promising candidates for photothermal therapy and should be investigated for efficient heat generation under biocompatible laser excitation. Particular attention needs to be devoted to the contact between materials to design and optimize the interface, facilitating successful energy transfer. Solving these mentioned scientific challenges will produce more sophisticated architectures with new functionalities for a broader range of applications.

AUTHOR INFORMATION

Corresponding Author

Hao Jing – Department of Chemistry and Biochemistry,
George Mason University, Fairfax, Virginia 22030, United States; orcid.org/0000-0002-6332-266X;
Email: hjing2@gmu.edu

Author

Mariia Ivanchenko – Department of Chemistry and Biochemistry, George Mason University, Fairfax, Virginia 22030, United States

Complete contact information is available at:

<https://pubs.acs.org/10.1021/acs.chemmater.3c00346>

Notes

The authors declare no competing financial interest.

ACKNOWLEDGMENTS

This work was supported by the Startup Foundation (170397-M18700-10502) and the College of Science (COS) Seed Grant (102284-M13877) of George Mason University.

REFERENCES

- (1) Younis, M. R.; Wang, C.; An, R. B.; Wang, S. J.; Younis, M. A.; Li, Z. Q.; Wang, Y.; Ihsan, A.; Ye, D. J.; Xia, X. H. Low Power Single Laser Activated Synergistic Cancer Phototherapy Using Photosensitizer Functionalized Dual Plasmonic Photothermal Nanoagents. *ACS Nano* **2019**, *13* (2), 2544–2557.
- (2) Tang, H.; Chen, Z. A.; Ouyang, C.; Ye, Z. R.; Li, S. B.; Hong, Z. L.; Zhi, M. J. Coupling the Surface Plasmon Resonance of WO_{3-x} and Au for Enhancing the Photocatalytic Activity of the Nonoxidative Methane Coupling Reaction. *J. Phys. Chem. C* **2022**, *126* (47), 20036–20048.
- (3) Chen, K.; Gong, L. L.; Ding, S. J.; Liu, J.; Ma, S.; Wang, J. H.; Yang, D. J.; Pan, G. M.; Hao, Z. H.; Zhou, L.; Wang, Q. Q. Tunable Charge Transfer and Dual Plasmon Resonances of $\text{Au}@ \text{WO}_{3-x}$ Hybrids and Applications in Photocatalytic Hydrogen Generation. *Plasmonics* **2020**, *15* (1), 21–29.
- (4) Zhu, H.; Wang, Y.; Chen, C.; Ma, M. R.; Zeng, J. F.; Li, S. Z.; Xia, Y. S.; Gao, M. Y. Monodisperse Dual Plasmonic $\text{Au}@ \text{Cu}_{2-x}\text{E}$ (E = S, Se) Core@Shell Supraparticles: Aqueous Fabrication, Multimodal Imaging, and Tumor Therapy at in Vivo Level. *ACS Nano* **2017**, *11* (8), 8273–8281.
- (5) Katyal, J.; Badoni, V. Localized Surface Plasmon Resonance and Field Enhancement of Au, Ag, Al and Cu Nanoparticles Having Isotropic and Anisotropic Nanostructure. *Mater. Today: Proc.* **2021**, *44*, 5012–5017.
- (6) Zhao, Y. X.; Pan, H. C.; Lou, Y. B.; Qiu, X. F.; Zhu, J. J.; Burda, C. Plasmonic Cu_{2-x}S Nanocrystals: Optical and Structural Properties of Copper-Deficient Copper(I) Sulfides. *J. Am. Chem. Soc.* **2009**, *131* (12), 4253–4261.
- (7) Luther, J. M.; Jain, P. K.; Ewers, T.; Alivisatos, A. P. Localized Surface Plasmon Resonances Arising from Free Carriers in Doped Quantum Dots. *Nat. Mater.* **2011**, *10* (5), 361–366.
- (8) Liu, X.; Swihart, M. T. Heavily-Doped Colloidal Semiconductor and Metal Oxide Nanocrystals: an Emerging New Class of Plasmonic Nanomaterials. *Chem. Soc. Rev.* **2014**, *43* (11), 3908–3920.
- (9) Shan, B. B.; Zhao, Y. W.; Li, Y. W.; Wang, H. T.; Chen, R.; Li, M. High-Quality Dual-Plasmonic $\text{Au}@ \text{Cu}_{2-x}\text{Se}$ Nanocrystals with Precise Cu_{2-x}Se Domain Size Control and Tunable Optical Properties in the Second Near-Infrared Biowindow. *Chem. Mater.* **2019**, *31* (23), 9875–9886.
- (10) Kimura, T.; Yao, H. Magnetic Circular Dichroism Study on Dual Plasmonic $\text{Au}@ \text{CuS}$ Core-Shell Nanoparticles: Effects of Shell Thickness and Uniformity. *J. Phys. Chem. C* **2022**, *126* (18), 7933–7940.
- (11) Li, Y. Y.; Pan, G. M.; Liu, Q. Y.; Ma, L.; Xie, Y.; Zhou, L.; Hao, Z. H.; Wang, Q. Q. Coupling Resonances of Surface Plasmon in Gold Nanorod/Copper Chalcogenide Core-Shell Nanostructures and Their Enhanced Photothermal Effect. *ChemPhysChem* **2018**, *19* (15), 1852–1858.
- (12) Hsu, S. W.; Bryks, W.; Tao, A. R. Effects of Carrier Density and Shape on the Localized Surface Plasmon Resonances of Cu_{2-x}S Nanodisks. *Chem. Mater.* **2012**, *24* (19), 3765–3771.
- (13) Ma, S.; Chen, K.; Qiu, Y. H.; Gong, L. L.; Pan, G. M.; Lin, Y. J.; Hao, Z. H.; Zhou, L.; Wang, Q. Q. Controlled Growth of $\text{CdS}-\text{Cu}_{2-x}\text{S}$ Lateral Heteroshells on Au Nanoparticles with Improved Photocatalytic Activity and Photothermal Efficiency. *J. Mater. Chem. A* **2019**, *7* (7), 3408–3414.
- (14) Zou, Y.; Sun, C.; Gong, W. B.; Yang, X. F.; Huang, X.; Yang, T.; Lu, W. B.; Jiang, J. Morphology-Controlled Synthesis of Hybrid Nanocrystals via a Selenium-Mediated Strategy with Ligand Shielding Effect: The Case of Dual Plasmonic $\text{Au}-\text{Cu}_{2-x}\text{Se}$. *ACS Nano* **2017**, *11* (4), 3776–3785.
- (15) Ding, X. G.; Liow, C. H.; Zhang, M. X.; Huang, R. J.; Li, C. Y.; Shen, H.; Liu, M. Y.; Zou, Y.; Gao, N.; Zhang, Z. J.; Li, Y. G.; Wang, Q. B.; Li, S. Z.; Jiang, J. Surface Plasmon Resonance Enhanced Light Absorption and Photothermal Therapy in the Second Near-Infrared Window. *J. Am. Chem. Soc.* **2014**, *136* (44), 15684–15693.
- (16) Bessel, P.; Niebur, A.; Kranz, D.; Lauth, J.; Dorfs, D. Probing Bidirectional Plasmon-Plasmon Coupling-Induced Hot Charge Carriers in Dual Plasmonic Au/CuS Nanocrystals. *Small* **2023**, *19*, 2370080.
- (17) Ivanchenko, M.; Nooshnab, V.; Myers, A. F.; Large, N.; Evangelista, A. J.; Jing, H. Enhanced Dual Plasmonic Photocatalysis through Plasmonic Coupling in Eccentric Noble Metal-Nonstoichiometric Copper Chalcogenide Hetero-Nanostructures. *Nano Res.* **2022**, *15* (2), 1579–1586.
- (18) Wang, H. T.; Li, M. Near-Infrared II Thermoplasmonics of Cuprous Selenide Multilayer Nanoshells: The Role of the Plasmonic Core. *J. Phys. Chem. Lett.* **2021**, *12* (20), 4928–4935.
- (19) Spear, N. J.; Hallman, K. A.; Hernandez-Pagan, E. A.; Davidson, R. B.; Arrowood, S. L.; Wistuba, A. L.; Tan, W. Z.; Haglund, R. F.; Macdonald, J. E. Enhanced Broadband and Harmonic Upconversion from Coupled Semiconductor and Metal Nanoparticle Films. *ACS Appl. Nano Mater.* **2020**, *3* (4), 3144–3150.
- (20) Spear, N. J.; Yan, Y. M.; Queen, J. M.; Singh, M. R.; Macdonald, J. E.; Haglund, R. F. Surface Plasmon Mediated Harmonically Resonant Effects on Third Harmonic Generation from Au and CuS Nanoparticle Films. *Nanophotonics* **2023**, *12* (2), 273–284.

- (21) Cao, P. F.; Liang, M. Y.; Wu, Y. Y.; Li, Y.; Cheng, L. New Hybridization Coupling Mechanism and Enhanced Sensitivity in a $\text{Cu}_{2-x}\text{S}@Au$ Nanoparticle Dimer. *Nanotechnology* **2020**, *31* (36), 365501.
- (22) Xia, Y. N.; Halas, N. J. Shape-Controlled Synthesis and Surface Plasmonic Properties of Metallic Nanostructures. *MRS Bull.* **2005**, *30* (5), 338–344.
- (23) Chen, X. J.; Cabello, G.; Wu, D. Y.; Tian, Z. Q. Surface-Enhanced Raman Spectroscopy toward Application in Plasmonic Photocatalysis on Metal Nanostructures. *J. Photochem. Photobiol. C: Photochem. Rev.* **2014**, *21*, 54–80.
- (24) Warren, S. C.; Thimsen, E. Plasmonic Solar Water Splitting. *Energy Environ. Sci.* **2012**, *5* (1), 5133–5146.
- (25) Willets, K. A.; Van Duyne, R. P. Localized Surface Plasmon Resonance Spectroscopy and Sensing. *Annu. Rev. Phys. Chem.* **2007**, *58*, 267–297.
- (26) Schuller, J. A.; Barnard, E. S.; Cai, W. S.; Jun, Y. C.; White, J. S.; Brongersma, M. L. Plasmonics for Extreme Light Concentration and Manipulation. *Nat. Mater.* **2010**, *9* (3), 193–204.
- (27) Singh, S.; Singh, P. K.; Umar, A.; Lohia, P.; Albargi, H.; Castaneda, L.; Dwivedi, D. K. 2D Nanomaterial-Based Surface Plasmon Resonance Sensors for Biosensing Applications. *Micro-machines* **2020**, *11* (8), 779.
- (28) Gutierrez, Y.; Brown, A. S.; Moreno, F.; Losurdo, M. Plasmonics Beyond Noble Metals: Exploiting Phase and Compositional Changes for Manipulating Plasmonic Performance. *J. Appl. Phys.* **2020**, *128* (8), 080901.
- (29) Shim, H.; Kuang, Z. Y.; Miller, O. D. Optical Materials for Maximal Nanophotonic Response. *Opt. Mater. Express* **2020**, *10* (7), 1561–1585.
- (30) Zhang, X. M.; Chen, Y. L.; Liu, R. S.; Tsai, D. P. Plasmonic Photocatalysis. *Rep. Prog. Phys.* **2013**, *76* (4), 046401.
- (31) Xu, W.; Liu, H. C.; Zhou, D. L.; Chen, X.; Ding, N.; Song, H. W.; Agren, H. Localized Surface Plasmon Resonances in Self-Doped Copper Chalcogenide Binary Nanocrystals and Their Emerging Applications. *Nano Today* **2020**, *33*, 100892.
- (32) Agrawal, A.; Cho, S. H.; Zandi, O.; Ghosh, S.; Johns, R. W.; Milliron, D. J. Localized Surface Plasmon Resonance in Semiconductor Nanocrystals. *Chem. Rev.* **2018**, *118* (6), 3121–3207.
- (33) Liu, M. X.; Xue, X. Z.; Ghosh, C.; Liu, X.; Liu, Y.; Furlani, E. P.; Swihart, M. T.; Prasad, P. N. Room-Temperature Synthesis of Covellite Nanoplatelets with Broadly Tunable Localized Surface Plasmon Resonance. *Chem. Mater.* **2015**, *27* (7), 2584–2590.
- (34) Li, W. H.; Zamani, R.; Gil, P. R.; Pelaz, B.; Ibanez, M.; Cadavid, D.; Shavel, A.; Alvarez-Puebla, R. A.; Parak, W. J.; Arbiol, J.; Cabot, A. CuTe Nanocrystals: Shape and Size Control, Plasmonic Properties, and Use as SERS Probes and Photothermal Agents. *J. Am. Chem. Soc.* **2013**, *135* (19), 7098–7101.
- (35) Guo, Q. B.; Yao, Y. H.; Luo, Z. C.; Qin, Z. P.; Xie, G. Q.; Liu, M.; Kang, J.; Zhang, S.; Bi, G.; Liu, X. F.; Qiu, J. R. Universal Near-Infrared and Mid-Infrared Optical Modulation for Ultrafast Pulse Generation Enabled by Colloidal Plasmonic Semiconductor Nanocrystals. *ACS Nano* **2016**, *10* (10), 9463–9469.
- (36) White, S. L.; Banerjee, P.; Jain, P. K. Liquid-Like Cationic Sub-Lattice in Copper Selenide Clusters. *Nat. Commun.* **2017**, *8*, 14514.
- (37) Liu, X.; Wang, X. L.; Zhou, B.; Law, W. C.; Cartwright, A. N.; Swihart, M. T. Size-Controlled Synthesis of Cu_{2-x}E ($\text{E} = \text{S}, \text{Se}$) Nanocrystals with Strong Tunable Near-Infrared Localized Surface Plasmon Resonance and High Conductivity in Thin Films. *Adv. Funct. Mater.* **2013**, *23* (10), 1256–1264.
- (38) Ha, M. J.; Kim, J. H.; You, M.; Li, Q.; Fan, C. H.; Nam, J. M. Multicomponent Plasmonic Nanoparticles: From Heterostructured Nanoparticles to Colloidal Composite Nanostructures. *Chem. Rev.* **2019**, *119* (24), 12208–12278.
- (39) Wang, B.; Li, R. R.; Guo, G.; Xia, Y. S. Janus and Core@Shell Gold Nanorod@ Cu_{2-x}S Supraparticles: Reactive Site Regulation Fabrication, Optical/Catalytic Synergetic Effects and Enhanced Photothermal Efficiency/Photostability. *Chem. Commun.* **2020**, *56* (63), 8996–8999.
- (40) Saruyama, M.; Sato, R.; Teranishi, T. Transformations of Ionic Nanocrystals via Full and Partial Ion Exchange Reactions. *Acc. Chem. Res.* **2021**, *54* (4), 765–775.
- (41) Li, X. Y.; Ji, M. W.; Li, H. B.; Wang, H. Z.; Xu, M.; Rong, H. P.; Wei, J.; Liu, J.; Liu, J. J.; Chen, W. X.; Zhu, C. Z.; Wang, J.; Zhang, J. T. Cation/Anion Exchange Reactions toward the Syntheses of Upgraded Nanostructures: Principles and Applications. *Matter* **2020**, *2* (3), 554–586.
- (42) Cao, Y. L.; Li, S.; Yu, X. D.; Li, W. H.; Bo, Z. S. Synthesis of Hybrid $\text{Au-Ag}_2\text{S-Cu}_{2-x}\text{S}$ Nanocrystals with Disparate Interfacial Features. *J. Colloid Interface Sci.* **2021**, *603*, 11–16.
- (43) Cho, G.; Park, Y.; Hong, Y. K.; Ha, D. H. Ion Exchange: an Advanced Synthetic Method for Complex Nanoparticles. *Nano Convergence* **2019**, *6*, 17 DOI: 10.1186/s40580-019-0187-0.
- (44) Sun, M. Q.; Fu, X. Q.; Chen, K. X.; Wang, H. Dual-Plasmonic Gold@Copper Sulfide Core-Shell Nanoparticles: Phase-Selective Synthesis and Multimodal Photothermal and Photocatalytic Behaviors. *ACS Appl. Mater. Interfaces* **2020**, *12* (41), 46146–46161.
- (45) Ding, X. G.; Zhao, H. T.; Li, C. Y.; Wang, Q. B.; Jiang, J. All-in-One Theranostic Nanoplatform with Controlled Drug Release and Activated MRI Tracking Functions for Synergistic NIR-II Hyperthermia-Chemotherapy of Tumors. *Nano Res.* **2019**, *12* (12), 2971–2981.
- (46) Li, X.; Cheng, Y.; Xu, J.; Lin, H.; Wang, Y. S. Utilizing Au-CuS Heterodimer to Intensify Upconversion Emission of $\text{NaGdF}_4:\text{Yb/Er}$ Nanocrystals. *J. Mater. Sci.* **2020**, *55* (16), 6891–6902.
- (47) Ma, L.; Chen, Y. L.; Yang, X.; Li, H. X.; Ding, S. J.; Hou, H. Y.; Xiong, L.; Qin, P. L.; Chen, X. B. Growth Behavior of Au/ Cu_{2-x}S Hybrids and Their Plasmon-Enhanced Dual-Functional Catalytic Activity. *CrystEngComm* **2019**, *21* (37), 5610–5617.
- (48) Motl, N. E.; Bondi, J. F.; Schaak, R. E. Synthesis of Colloidal Au-Cu₂S Heterodimers via Chemically Triggered Phase Segregation of AuCu Nanoparticles. *Chem. Mater.* **2012**, *24* (9), 1552–1554.
- (49) Ding, X. G.; Zou, Y.; Jiang, J. Au-Cu₂S Heterodimer Formation via Oxidization of AuCu alloy Nanoparticles and in situ Formed Copper Thiolate. *J. Mater. Chem.* **2012**, *22* (43), 23169–23174.
- (50) Sun, M. Q.; Wang, Z. X.; Wang, H. Chemically Driven Phase Segregation of Alloy Nanoparticles: A Versatile Route to Dual-Plasmonic Gold@Copper Chalcogenide Heteronanostructures. *Chem. Mater.* **2022**, *34* (4), 1965–1975.
- (51) Das, A.; Arunagiri, V.; Tsai, H. C.; Prasanna, A.; Moirangthem, R. S. Core-Multishell Au@ $\text{Cu}_{2-x}\text{S}@Au$ Nanoparticles for Surface-Enhanced Raman Scattering-Guided Low-Intensity Photothermal Cancer Therapy. *ACS Appl. Nano Mater.* **2021**, *4* (11), 12278–12288.
- (52) Liu, X.; Lee, C.; Law, W. C.; Zhu, D. W.; Liu, M. X.; Jeon, M.; Kim, J.; Prasad, P. N.; Kim, C.; Swihart, M. T. Au-Cu_{2-x}Se Heterodimer Nanoparticles with Broad Localized Surface Plasmon Resonance as Contrast Agents for Deep Tissue Imaging. *Nano Lett.* **2013**, *13* (9), 4333–4339.
- (53) Zhang, L.; Jiang, C. J.; Li, B.; Liu, Z. W.; Gu, B. X.; He, S. M.; Li, P. L.; Sun, Y.; Song, S. L. A Core-Shell Au@ Cu_{2-x}Se Heterogeneous Metal Nanocomposite for Photoacoustic and Computed Tomography Dual-Imaging-Guided Photothermal Boosted Chemodynamic Therapy. *J. Nanobiotechnology* **2021**, *19* (1), 410.
- (54) Shan, B. B.; Liu, H. Y.; Li, L. H.; Lu, Y. X.; Li, M. Near-Infrared II Plasmonic Phototheranostics with Glutathione Depletion for Multimodal Imaging-Guided Hypoxia-Tolerant Chemodynamic-Photocatalytic-Photothermal Cancer Therapy Triggered by a Single Laser. *Small* **2022**, *18* (4), 2105638.
- (55) Sen, S.; Shyamal, S.; Mehetor, S. K.; Sahu, P.; Pradhan, N. Au-Cu_{2-x}Te Plasmonic Heteronanostructure Photoelectrocatalysts. *J. Phys. Chem. Lett.* **2021**, *12* (47), 11585–11590.
- (56) Das, A.; Arunagiri, V.; Tsai, H. C.; Prasanna, A.; Lai, J. Y.; Da-Hong, P.; Moirangthem, R. S. Investigation of Dual Plasmonic Core-Shell Ag@CuS Nanoparticles for Potential Surface-Enhanced Raman Spectroscopy-Guided Photothermal Therapy. *Nanomedicine* **2021**, *16* (11), 909–923.

- (57) Jiang, R. B.; Chen, H. J.; Shao, L.; Li, Q.; Wang, J. F. Unraveling the Evolution and Nature of the Plasmons in (Au Core)-(Ag Shell) Nanorods. *Adv. Mater.* **2012**, *24* (35), 200–207.
- (58) Millstone, J. E.; Wei, W.; Jones, M. R.; Yoo, H. J.; Mirkin, C. A. Iodide Ions Control Seed-Mediated Growth of Anisotropic Gold Nanoparticles. *Nano Lett.* **2008**, *8* (8), 2526–2529.
- (59) Wang, W.; Ma, S.; Chen, K.; Wang, P. F.; Liu, Q. Y.; Zhou, L.; Wang, Q. Q. Controlled Growth of Cu_{2-x}S Sheet-Like Nanoshells and Cu_{2-x}S -CdS p-n Junctions on Au Nanorods with Coupled Plasmon Resonances and Enhanced Photocatalytic Activities. *J. Mater. Chem. C* **2020**, *8* (9), 3058–3068.
- (60) Leng, C. B.; Zhang, X.; Xu, F. X.; Yuan, Y.; Pei, H.; Sun, Z. H.; Li, L.; Bao, Z. H. Engineering Gold Nanorod-Copper Sulfide Heterostructures with Enhanced Photothermal Conversion Efficiency and Photostability. *Small* **2018**, *14* (12), 1703077.
- (61) Ji, M. W.; Xu, M.; Zhang, W.; Yang, Z. Z.; Huang, L.; Liu, J. J.; Zhang, Y.; Gu, L.; Yu, Y. X.; Hao, W. C.; An, P. F.; Zheng, L. R.; Zhu, H. S.; Zhang, J. T. Structurally Well-Defined $\text{Au}@_{\text{Cu}_{2-x}\text{S}}$ Core-Shell Nanocrystals for Improved Cancer Treatment Based on Enhanced Photothermal Efficiency. *Adv. Mater.* **2016**, *28* (16), 3094–3101.
- (62) Muhammed, M. A. H.; Doblinger, M.; Rodriguez-Fernandez, J. Switching Plasmons: Gold Nanorod-Copper Chalcogenide Core-Shell Nanoparticle Clusters with Selectable Metal/Semiconductor NIR Plasmon Resonances. *J. Am. Chem. Soc.* **2015**, *137* (36), 11666–11677.
- (63) Shan, B. B.; Wang, H. T.; Li, L. H.; Zhou, G. Z.; Wen, Y.; Chen, M. Y.; Li, M. Rationally Designed Dual-Plasmonic Gold Nanorod@ Cuprous Selenide Hybrid Heterostructures by Regioselective Overgrowth for in vivo Photothermal Tumor Ablation in the Second Near-Infrared Biowindow. *Theranostics* **2020**, *10* (25), 11656–11672.
- (64) Tang, L.; Liang, S.; Li, J. B.; Zhang, D.; Chen, W. B.; Yang, Z. J.; Xiao, S.; Wang, Q. Q. Controlled Synthesis of Au Nanocrystals-Metal Selenide Hybrid Nanostructures toward Plasmon-Enhanced Photoelectrochemical Energy Conversion. *Nanomater.* **2020**, *10* (3), 564.
- (65) Cao, P. F.; Chen, H. Z.; Zhang, H. L.; Cheng, L.; Niu, T. M. High-Sensitivity Refractive Index of $\text{Au}@_{\text{Cu}_{2-x}\text{S}}$ Core-Shell Nanorods. *RSC Adv.* **2018**, *8* (61), 35005–35013.
- (66) Ivanchenko, M.; Jing, H. Anisotropic Dual-Plasmonic Hetero-Nanostructures with Tunable Plasmonic Coupling Effects. *Nanoscale Adv.* **2022**, *4* (12), 2632–2636.
- (67) Wu, J. Y.; Lai, T. H.; Fang, M. J.; Chen, J. Y.; Kuo, M. Y.; Chiu, Y. H.; Hsieh, P. Y.; Tsao, C. W.; Chang, H. E.; Chang, Y. P.; Wang, C. Y.; Chen, C. Y.; Sone, M.; Wu, W. W.; Chang, T. F. M.; Hsu, Y. J. Electronic Interactions and Charge-Transfer Dynamics for a Series of Yolk-Shell Nanocrystals: Implications for Photocatalysis. *ACS Appl. Nano Mater.* **2022**, *5* (6), 8404–8416.
- (68) Tu, W. G.; Zhou, Y.; Li, H. J.; Li, P.; Zou, Z. G. $\text{Au}@_{\text{TiO}_2}$ Yolk-Shell Hollow Spheres for Plasmon-Induced Photocatalytic Reduction of CO_2 to Solar Fuel via a Local Electromagnetic Field. *Nanoscale* **2015**, *7* (34), 14232–14236.
- (69) Zhang, J.; Liu, G. G.; He, F.; Chen, L. X.; Huang, Y. $\text{Au}@_{\text{Cu}_7\text{S}_4}$ Yolk-Shell Nanoparticles as a 980 nm Laser-Driven Photothermal Agent with a Heat Conversion Efficiency of 63%. *RSC Adv.* **2015**, *5* (107), 87903–87907.
- (70) Cao, Y.; Li, S. Z.; Chen, C.; Wang, D. D.; Wu, T. T.; Dong, H. F.; Zhang, X. J. Rattle-Type $\text{Au}@_{\text{Cu}_{2-x}\text{S}}$ Hollow Mesoporous Nanocrystals with Enhanced Photothermal Efficiency for Intracellular Oncogenic microRNA Detection and Chemo-Photothermal Therapy. *Biomaterials* **2018**, *158*, 23–33.
- (71) Ji, M. W.; Li, X. Y.; Wang, H. Z.; Huang, L.; Xu, M.; Liu, J.; Liu, J. J.; Wang, J.; Zhang, J. T. Versatile Synthesis of Yolk/Shell Hybrid Nanocrystals via Ion-Exchange Reactions for Novel Metal/Semiconductor and Semiconductor/Semiconductor Conformations. *Nano Res.* **2017**, *10* (9), 2977–2987.
- (72) Yu, X. J.; Bi, J. L.; Yang, G.; Tao, H. Z.; Yang, S. C. Synergistic Effect Induced High Photothermal Performance of Au Nanorod@ Cu_7S_4 Yolk-Shell Nanooctahedron Particles. *J. Phys. Chem. C* **2016**, *120* (43), 24533–24541.
- (73) Chang, Y.; Cheng, Y.; Feng, Y. L.; Jian, H.; Wang, L.; Ma, X. M.; Li, X.; Zhang, H. Y. Resonance Energy Transfer-Promoted Photothermal and Photodynamic Performance of Gold-Copper Sulfide Yolk-Shell Nanoparticles for Chemophototherapy of Cancer. *Nano Lett.* **2018**, *18* (2), 886–897.
- (74) Ivanchenko, M.; Carroll, A. L.; Brothers, A. B.; Jing, H. Facile Aqueous Synthesis of Hollow Dual Plasmonic Hetero-Nanostructures with Tunable Optical Responses through Nanoscale Kirkendall Effects. *Nanoscale Adv.* **2022**, *5*, 88–95.
- (75) Hu, C.; Chen, W. H.; Xie, Y.; Verma, S. K.; Destro, P.; Zhan, G.; Chen, X. Z.; Zhao, X. J.; Schuck, P. J.; Kriegel, I.; Manna, L. Generating Plasmonic Heterostructures by Cation Exchange and Redox Reactions of Covellite CuS Nanocrystals with Au^{3+} Ions. *Nanoscale* **2018**, *10* (6), 2781–2789.
- (76) Deng, X. R.; Li, K.; Cai, X. C.; Liu, B.; Wei, Y.; Deng, K. R.; Xie, Z. X.; Wu, Z. J.; Ma, P. A.; Hou, S. Y.; Cheng, Z. Y.; Lin, J. A. Hollow-Structured $\text{CuS}@_{\text{Cu}_2\text{S}}@_{\text{Au}}$ Nanohybrid: Synergistically Enhanced Photothermal Efficiency and Photoswitchable Targeting Effect for Cancer Theranostics. *Adv. Mater.* **2017**, *29* (36), 1701266.
- (77) Lv, Q.; Gao, M. Y.; Cheng, Z. H.; Chen, Q.; Shen, A. G.; Hu, J. M. Rational Synthesis of Hollow Cubic $\text{CuS}@_{\text{Spiky Au}}$ Core-Shell Nanoparticles for Enhanced Photothermal and SERS Effects. *Chem. Commun.* **2018**, *54* (95), 13399–13402.
- (78) Tsangas, T.; Ruhmlieb, C.; Hentschel, S.; Noei, H.; Stierle, A.; Kipp, T.; Mews, A. Controlled Growth of Gold Nanoparticles on Covellite Copper Sulfide Nanoplatelets for the Formation of Plate-Satellite Hybrid Structures. *Chem. Mater.* **2022**, *34* (3), 1157–1166.
- (79) Basu, M.; Nazir, R.; Fageria, P.; Pande, S. Construction of CuS/Au Heterostructure through a Simple Photoreduction Route for Enhanced Electrochemical Hydrogen Evolution and Photocatalysis. *Sci. Rep.* **2016**, *6*, 34738.
- (80) Wang, Z. J.; Yu, N.; Li, X.; Yu, W. J.; Han, S. L.; Ren, X. L.; Yin, S. W.; Li, M. Q.; Chen, Z. G. Galvanic Exchange-Induced Growth of Au Nanocrystals on CuS Nanoplates for Imaging Guided Photothermal Ablation of Tumors. *Chem. Eng. J.* **2020**, *381*, 122613.
- (81) Ma, L.; Yang, D. J.; Song, X. P.; Li, H. X.; Ding, S. J.; Xiong, L.; Qin, P. L.; Chen, X. B. Pt Decorated (Au Nanosphere)/(CuSe Ultrathin Nanoplate) Tangential Hybrids for Efficient Photocatalytic Hydrogen Generation via Dual-Plasmon-Induced Strong VIS-NIR Light Absorption and Interfacial Electric Field Coupling. *Sol. RRL* **2020**, *4* (1), 1900376.
- (82) Wang, X. W.; Zhong, X. Y.; Lei, H. L.; Geng, Y. H.; Zhao, Q.; Gong, F.; Yang, Z. J.; Dong, Z. L.; Liu, Z.; Cheng, L. Hollow Cu_2Se Nanozymes for Tumor Photothermal-Catalytic Therapy. *Chem. Mater.* **2019**, *31* (16), 6174–6186.
- (83) Yu, H. L.; He, M. T.; Li, Y. C.; Liu, Y. H.; Xu, Z. G.; Zhang, L.; Kang, Y. J.; Xue, P. A Robust $\text{Au}@_{\text{Cu}_{2-x}\text{S}}$ Nanoreactor Assembled by Silk Fibroin for Enhanced Intratumoral Glucose Depletion and Redox Dyshomeostasis. *Biomaterials* **2023**, *293*, 121970.
- (84) Hu, C. L.; Zhang, Z. X.; Liu, S. N.; Liu, X. J.; Pang, M. L. Monodispersed CuSe Sensitized Covalent Organic Framework Photosensitizer with an Enhanced Photodynamic and Photothermal Effect for Cancer Therapy. *ACS Appl. Mater. Interfaces* **2019**, *11* (26), 23072–23082.
- (85) Zhang, H.; Wang, T. T.; Qiu, W. B.; Han, Y. B.; Sun, Q.; Zeng, J. F.; Yan, F.; Zheng, H. R.; Li, Z.; Gao, M. Y. Monitoring the Opening and Recovery of the Blood-Brain Barrier with Noninvasive Molecular Imaging by Biodegradable Ultrasmall Cu_{2-x}Se Nanoparticles. *Nano Lett.* **2018**, *18* (8), 4985–4992.
- (86) Wang, Y. L.; Li, Z. L.; Hu, Y.; Liu, J.; Guo, M. Y.; Wei, H. X.; Zheng, S. L.; Jiang, T. T.; Sun, X.; Ma, Z.; Sun, Y.; Besenbacher, F.; Chen, C. Y.; Yu, M. Photothermal Conversion-Coordinated Fenton-Like and Photocatalytic Reactions of $\text{Cu}_{2-x}\text{Se}-\text{Au}$ Janus Nanoparticles for Tri-Combination Antitumor Therapy. *Biomaterials* **2020**, *255*, 120167.
- (87) Huang, Q.; Zhang, S. H.; Zhang, H.; Han, Y. B.; Liu, H. H.; Ren, F.; Sun, Q.; Li, Z.; Gao, M. Y. Boosting the Radiosensitizing and Photothermal Performance of Cu_{2-x}Se Nanocrystals for Synergistic

Radiophotothermal Therapy of Orthotopic Breast Cancer. *ACS Nano* **2019**, *13* (2), 1342–1353.

(88) Wan, X. D.; Xu, M.; Huang, L.; Tu, G. P.; Ji, M. W.; Su, M. Y.; Li, Y. M.; Li, X. Y.; Wang, H. Z.; Zhang, J. T. Positively Charged Collective Oscillations Induce Efficient A β 1–42 Fibril Degradation in the Presence of Novel Au@Cu_{2-x}S Core/Shell Nanorods. *Chem. Commun.* **2021**, *57* (52), 6384–6387.

(89) Lv, Q.; Min, H.; Duan, D. B.; Fang, W.; Pan, G. M.; Shen, A. G.; Wang, Q. Q.; Nie, G. J.; Hu, J. M. Total Aqueous Synthesis of Au@Cu_{2-x}S Core-Shell Nanoparticles for In Vitro and In Vivo SERS/PA Imaging-Guided Photothermal Cancer Therapy. *Adv. Health. Mater.* **2018**, *8* (2), 1801257.

(90) Wu, T.; Wang, Z. C.; Xiao, L.; Qin, P. L.; Qin, Z. L.; Ma, L.; Zeng, W.; Chen, X. B.; Xiong, L. B.; Fang, G. J. Mesoporous Au@Cu_{2-x}S Core-Shell Nanoparticles with Double Localized Surface Plasmon Resonance and Ligand Modulation for Hole-Selective Passivation in Perovskite Solar Cells. *Sol. RRL* **2021**, *5* (9), 2100358.

(91) Yang, Y.; Liu, J. Y.; Fu, Z. W.; Qin, D. Galvanic Replacement-Free Deposition of Au on Ag for Core-Shell Nanocubes with Enhanced Chemical Stability and SERS Activity. *J. Am. Chem. Soc.* **2014**, *136* (23), 8153–8156.

(92) Garcia-Herrera, L. F.; McAllister, H. P.; Xiong, H. Y.; Wang, H. Y.; Lord, R. W.; O'Boyle, S. K.; Imamovic, A.; Steimle, B. C.; Schaak, R. E.; Plass, K. E. Multistep Regioselectivity and Non-Kirkendall Anion Exchange of Copper Chalcogenide Nanorods. *Chem. Mater.* **2021**, *33* (10), 3841–3850.

(93) Espinosa, A. R.; Novak, M.; Luo, Q.; Hole, B.; Doligon, C.; Sosa, K. P.; Gray, J. L.; Rossi, D. P.; Plass, K. E. Heterostructures of Cu_{2-x}S/Cu_{2-x}Te Plasmonic Semiconductors: Disappearing and Reappearing LSPR with Anion Exchange. *Chem. Commun.* **2022**, *58* (70), 9810–9813.

(94) Sen, S.; Bera, S.; Pradhan, N. Maneuvering Tellurium Chemistry to Design Metal-Telluride Heterostructures for Diverse Applications. *Chem. Mater.* **2022**, *34* (21), 9329–9343.

(95) Xu, W. J.; Jia, J.; Wang, T.; Li, C.; He, B. W.; Zong, J. P.; Wang, Y. W.; Fan, H. J.; Xu, H. X.; Feng, Y. H.; Chen, H. Y. Continuous Tuning of Au-Cu₂O Janus Nanostructures for Efficient Charge Separation. *Angew. Chem., Int. Ed.* **2020**, *59* (49), 22246–22251.

(96) Zhang, L.; Jing, H.; Boisvert, G.; He, J. Z.; Wang, H. Geometry Control and Optical Tunability of Metal-Cuprous Oxide Core-Shell Nanoparticles. *ACS Nano* **2012**, *6* (4), 3514–3527.

(97) Hong, J. W.; Wi, D. H.; Lee, S. U.; Han, S. W. Metal-Semiconductor Heteronanocrystals with Desired Configurations for Plasmonic Photocatalysis. *J. Am. Chem. Soc.* **2016**, *138* (48), 15766–15773.

(98) Zhang, Y. C.; He, S.; Guo, W. X.; Hu, Y.; Huang, J. W.; Mulcahy, J. R.; Wei, W. D. Surface-Plasmon-Driven Hot Electron Photochemistry. *Chem. Rev.* **2018**, *118* (6), 2927–2954.

(99) Qi, P.; Gao, X. X.; Wang, J.; Liu, H. M.; He, D. H.; Zhang, Q. J. A Minireview on Catalysts for Photocatalytic N₂ Fixation to Synthesize Ammonia. *RSC Adv.* **2022**, *12* (3), 1244–1257.

(100) Dunklin, J. R.; Rose, A. H.; Zhang, H. Y.; Miller, E. M.; van de Lagemaat, J. Plasmonic Hot Hole Transfer in Gold Nanoparticle-Decorated Transition Metal Dichalcogenide Nanosheets. *ACS Photonics* **2020**, *7* (1), 197–202.

(101) Lian, Z.; Sakamoto, M.; Matsunaga, H.; Vequizo, J. J. M.; Yamakata, A.; Haruta, M.; Kurata, H.; Ota, W.; Sato, T.; Teranishi, T. Near Infrared Light Induced Plasmonic Hot Hole Transfer at a Nano-Heterointerface. *Nat. Commun.* **2018**, *9* (1), 2314.

(102) Liu, X.; Wang, X. L.; Swihart, M. T. Cu_{2-x}S_{1-y}Se_y Alloy Nanocrystals with Broadly Tunable Near-Infrared Localized Surface Plasmon Resonance. *Chem. Mater.* **2013**, *25* (21), 4402–4408.

(103) Li, H.; Shibuta, M.; Yamada, T.; Hojo, H.; Kato, H. S.; Teranishi, T.; Sakamoto, M. Band Engineering-Tuned Localized Surface Plasmon Resonance in Diverse-Phased Cu_{2-x}S_ySe_{1-y} Nanocrystals. *J. Phys. Chem. C* **2022**, *126* (18), 8107–8112.

(104) Thompson; Katzbaer, R. R.; Terrones, M.; Schaak, R. E. Formation and Transformation of Cu_{2-x}Se_{1-y}Te_y Nanoparticles

Synthesized by Tellurium Anion Exchange of Copper Selenide. *Inorg. Chem.* **2023**, *62* (11), 4550–4557.

(105) van der Stam, W.; Berends, A. C.; de Mello Donega, C. Prospects of Colloidal Copper Chalcogenide Nanocrystals. *ChemPhysChem* **2016**, *17* (5), 559–581.

(106) Niezgodza, J. S.; Harrison, M. A.; McBride, J. R.; Rosenthal, S. J. Novel Synthesis of Chalcopyrite Cu₃In₇S₂ Quantum Dots with Tunable Localized Surface Plasmon Resonances. *Chem. Mater.* **2012**, *24* (16), 3294–3297.

(107) Coughlan, C.; Ibanez, M.; Dobrozhan, O.; Singh, A.; Cabot, A.; Ryan, K. M. Compound Copper Chalcogenide Nanocrystals. *Chem. Rev.* **2017**, *117* (9), 5865–6109.

(108) Anker, J. N.; Hall, W. P.; Lyandres, O.; Shah, N. C.; Zhao, J.; Van Duyne, R. P. Biosensing with Plasmonic Nanosensors. *Nat. Mater.* **2008**, *7* (6), 442–453.

(109) Lane, L. A.; Qian, X. M.; Nie, S. M. SERS Nanoparticles in Medicine: From Label-Free Detection to Spectroscopic Tagging. *Chem. Rev.* **2015**, *115* (19), 10489–10529.

(110) Gan, X. Y.; Keller, E. L.; Warkentin, C. L.; Crawford, S. E.; Frontiera, R. R.; Millstone, J. E. Plasmon-Enhanced Chemical Conversion Using Copper Selenide Nanoparticles. *Nano Lett.* **2019**, *19* (4), 2384–2388.

(111) Xu, Y.; Yu, S.; Tong, F.; Wang, Z.; Wang, P.; Liu, Y.; Cheng, H.; Fan, Y.; Wei, W.; Dai, Y.; Zheng, Z.; Huang, B. Dual-Plasmon-Enhanced Nitrophenol Hydrogenation over W₁₈O₄₉-Au Heterostructures Studied at the Single-Particle Level. *Catal. Sci. Technol.* **2023**, *13*, 1301–1310.

(112) Wang, L.; Wang, S. Y.; Mei, L.; Sun, J.; Shi, F.; Zhang, N.; Jiang, R. B. Nanostructures Composed of Dual Plasmonic Materials Exhibiting High Thermal Stability and SERS Enhancement. *Part Part Syst. Charact* **2021**, *38* (4), 2000321.

(113) Liu, J. X.; He, H. L.; Xiao, D.; Yin, S. T.; Ji, W.; Jiang, S. Z.; Luo, D.; Wang, B.; Liu, Y. J. Recent Advances of Plasmonic Nanoparticles and their Applications. *Materials* **2018**, *11* (10), 1833.

(114) Mendez-Gonzalez, D.; Melle, S.; Calderon, O. G.; Laurenti, M.; Cabrera-Granado, E.; Egatz-Gomez, A.; Lopez-Cabarcos, E.; Rubio-Retama, J.; Diaz, E. Control of Upconversion Luminescence by Gold Nanoparticle Size: from Quenching to Enhancement. *Nanoscale* **2019**, *11* (29), 13832–13844.

(115) Zhou, D. L.; Liu, D. L.; Xu, W.; Yin, Z.; Chen, X.; Zhou, P. W.; Cui, S. B.; Chen, Z. G.; Song, H. W. Observation of Considerable Upconversion Enhancement Induced by Cu_{2-x}S Plasmon Nanoparticles. *ACS Nano* **2016**, *10* (5), 5169–5179.